FERMILAB PROPOSAL NO. 454

Scientific Spokesman: Z.G.T. Guiragossián
High Energy Physics Laboratory
W.W. Hansen Laboratories of Physics
Stanford University
Stanford, California 94305
Telephone: (415) 497-0133

FERMILAB PROPOSAL

For An

EXPERIMENT TO MEASURE DEEP INELASTIC ELECTRON SCATTERING ON HYDROGEN AND DEUTERIUM WITH SEPARATION OF νW_2 AND W_1 NUCLEON STRUCTURE FUNCTIONS, AT THE HIGHEST FERMILAB ENERGIES AND Q^2 REGIONS

Submitted By

G. Conger, J. Edighoffer, A. Grigorian, Z. G. T. Guiragossián,
R. Hofstadter, T. P. McPharlin and M. R. Yearian

The W.W. Hansen High Energy Physics Laboratory and Department of Physics
Stanford University, Stanford, California 94305

and

B. C. Cox and J. Peoples, Jr.
The Fermi National Accelerator Laboratory
Batavia, Illinois 60510

October 15, 1975

TABLE OF CONTENTS

ABSTRACT

We propose to measure the inclusive deep inelastic electron-nucleon scattering cross sections on hydrogen and deuterium. Cross sections will be measured in the range of momentum transfers $Q^2_{min} = 0.160\ (GeV/c)^2$ and $Q^2_{max} = 160.0\ (GeV/c)^2$, in the range of recoil hadronic mass squared of $W^2_{min} = 2\ GeV^2$ and $W^2_{max} = 450\ GeV^2$. The electromagnetic structure functions, $\nu W_2(Q^2,\nu)$ and $W_1(Q^2,\nu)$, of both protons and neutrons will be measured and separated by well-known methods, in the highest possible unexplored FERMILAB kinematical regions.

The high intensity Proton-West superconducting beam will be used to yield an electron beam of high purity, based on a synchrotron radiation compensated tuning technique. The electron beam will be used at 150 GeV $(5 \times 10^8\ e^{\pm}/pulse)$, at 175 GeV $(3.6 \times 10^8\ e^{\pm}/pulse)$ and at 250 GeV $(1 \times 10^8\ e^{\pm}/pulse)$.

The scattered electron will be detected with good acceptance, good resolution and excellent identification. The detector will be the E-192 apparatus with small additions. A simple self-calibration procedure is available, both in experiment and apparatus, removing beam-associated and target-associated background in the entire (Q^2, W^2) kinematical regions. Usually, interesting physics occurs where counting rates are small. This experiment will be completely trustworthy in such regions because our apparatus provides excellent information on the tracking and identification of scattered electrons.

I. INTRODUCTION

The inclusive deep inelastic electron-nucleon scattering process has revealed exciting and new knowledge on the constituent nature of protons and neutrons. This knowledge is acquired by measuring the electromagnetic structure functions $\nu W_2^{p,n}$ and $W_1^{p,n}$ in terms of the variables (Q^2, W^2) or (Q^2, ν), where Q^2 is the invariant four-momentum transfer of electrons, $Q^2 = 4 E_o E' \sin^2(\theta/2)$, W is the effective mass of final state hadrons and $\nu = E_o - E'$ is the energy transfer by electrons. These variables are related by $W^2 = 2 M \nu - Q^2 + M^2$. It has been observed at SLAC energies that these structure functions depend only on a single scaling variable, such as $\omega = 2 M \nu/Q^2$ or $\omega' = 1 + W^2/Q^2$, in the deep inelastic scattering region. In nucleon constituent models, scaling behavior is interpreted as being a consequence of scattering off point-like constituents. Moreover, distinction is made in that the form factor νW_2 is a probe of parton distribution functions of both spin 0 and spin 1/2 constituents whereas the form factor W_1 is related to only parton distribution functions of spin 1/2 partons. Thus, measurement of both inelastic form factors νW_2 and W_1 <u>is</u> essential.

At a new kinematical domain,which we refer to as the FERMILAB region, it is crucial to discover if this scaling of the nucleon structure functions νW_2 and W_1 persists. In which region of (Q^2, W^2) is scaling valid; in what form does scaling breakdown occur; are there any threshold

effects due to, for example, the production of charmed matter; what are the shapes of νW_2 and W_1 at $\omega' = 2$ and at $\omega' = 1000$, etc. ? The determination of the shape of νW_2 and W_1 for protons and neutrons in terms of kinematical variables (Q^2, W^2) is a fundamental way of making observations of the constituent structure of nucleons.

We propose to answer these questions experimentally by measuring inclusive deep inelastic electron scattering cross sections on hydrogen and deuterium targets at electron beam energies of E_o = 150 GeV, 175 GeV and 250 GeV. With E_{proton} = 400 - 480 GeV the electron beam intensities are in the range of 10^9 - 10^8 $e^{\pm}$/pulse/10^{13} incident protons, making possible the detection of scattered electrons in our apparatus in the range of $Q^2_{min} = 0.16$ $(GeV/c)^2$ and $Q^2_{max} = 160.0$ $(GeV/c)^2$ and in the range of $W^2_{min} = 2$ GeV^2 and $W^2_{max} = 450.0$ GeV^2 . Also, at these energies, in a given (Q^2, W^2) domain the polarization parameter ϵ is sufficiently different, varying between $\epsilon = 0$ and $\epsilon = 1$, so that separation of the structure functions νW_2 and W_1 is made available by well-known techniques.

This experiment is made efficiently and economically possible at FERMILAB by the use of a simple conversion of a high intensity pion beam to produce a high intensity and good quality electron beam, and by the use of the apparatus of E-192 at the Proton-West Experimental Hall.

II. THE PHYSICS OBJECTIVE

The main thrust of this experiment is to measure the inclusive deep inelastic electron-proton and electron-neutron cross sections thereby determining the nucleon electromagnetic structure functions νW_2^p , W_1^p and νW_2^n , W_1^n in a new and unexplored kinematical domain, using a well-known separation technique. To be able to do this, it is necessary that scattered electrons be detected with large acceptance, good resolution and excellent identification in the presence of target-associated or beam-associated background. Moreover, it is necessary that both experiment and apparatus include a self-calibration scheme which can be performed efficiently and in short runs. Finally, statistical accuracy, systematic uncertainties and apparatus resolution should be well matched so that cross sections can be determined with over all errors in the range of 1.5% to 10% as Q^2 increases to extraordinarily high values.

In the one-photon-exchange Born approximation the inclusive electron-nucleon inelastic scattering cross section is expressed by:

$$\frac{d\sigma}{dE'd\Omega} = \left[\frac{2\,\alpha\,E'\cos\theta/2}{Q^2}\right]^2 \left\{W_2(\nu,Q^2) + 2(\tan^2\theta/2)W_1(\nu,Q^2)\right\} \qquad (1)$$

$$\frac{d\sigma}{dW^2dQ^2} = \frac{\pi}{2\,ME_o\,E'}\,\frac{d\sigma}{dE'd\Omega} \quad .$$

An equivalent representation is given in terms of the virtual photon flux Γ and the virtual photon cross sections with transverse

and longitudinal polarization modes,

$$\sigma_T(Q^2, W^2) \quad \text{and} \quad \sigma_L(Q^2, W^2):$$

$$\frac{d\sigma}{dE'\, d\Omega} = \Gamma\,(\sigma_T + \epsilon\,\sigma_L) \tag{2}$$

$$\Gamma = \frac{\alpha}{4\pi^2} \cdot \frac{E'}{E} \cdot \frac{K}{Q^2} \cdot \frac{2}{1-\epsilon}$$

so that the structure functions are related to the virtual photon cross sections:

$$W_1 = \frac{K}{M^2}\ \sigma_T/\sigma_o\ , \quad W_2 = \frac{K}{M^2} \cdot \frac{1}{1+\nu^2/Q^2} \cdot (\sigma_T + \sigma_L)/\sigma_o \tag{3}$$

where $\sigma_o = 4\pi^2\,\alpha/M^2 = 127\ \mu b$ and $K = (W^2 - M^2)/2M$.
In Eq. (2), $\epsilon(E_o, Q^2, W^2)$ is the polarization parameter, varying between $\epsilon = 0$ and $\epsilon = 1$. Comparing equation (2) and (3), it is seen that a measurement of inclusive electron-nucleon cross section $d\sigma/dE'd\Omega$ at $\epsilon = 0$ is a measurement of the structure function W_1 , and similarly a determination of $d\sigma/dE'd\Omega$ at $\epsilon = 1$ is a determination of the structure function W_2 . Thus, separation of W_2 and W_1 can be made in a given (Q^2, W^2) region, provided that cross sections $d\sigma/dQ^2dW^2$ are measured in the same region at several ϵ values, covering a good

lever arm between $\epsilon = 0$ and $\epsilon = 1$. In practice it is found that a 3-point measurement in a given (Q^2,W^2) region is sufficient to make an extrapolation to $\epsilon = 0$ and $\epsilon = 1$, and moreover a 2-point measurement is found to be adequate in neighboring regions.

The variation of the polarization parameter as a function of beam energies is shown in Figure 1, with entries given for 150 GeV, 175 GeV and 250 GeV in the (Q^2,W^2) FERMILAB region. The entries in each cell are given in the respective beam energy order. In this figure, both 3-point and 2-point separation zones are indicated, showing a great potential of acquiring new knowledge about the behavior of separated structure functions W_2 and W_1 at extremely large values of Q^2 and W^2 relative to the indicated SLAC region.

It is the good resolution of our apparatus and the nature of our electron experiment, which is relatively free of multiple scattering degradation, that permits the separation of structure functions, W_2 and W_1 in the fine grid of Q^2 and W^2, shown in Figure 1. Thus, the variation of W_2 and W_1 as a function of Q^2 and W^2 can be determined precisely. Without this inherent resolution such a fine binning of acquired data would not be meaningful.

Furthermore, the global acceptance of our apparatus in the (Q^2, W^2) plane eliminates the need of interpolation between (Q^2,W^2) neighboring data points for the separation and study of variation of W_2 and W_1 form factors. Such interpolation was required in small acceptance experiments in the SLAC region.

Finally, we summarize the present situation on the question of scaling. Recent experiments from SLAC produced determinations[1] of the four nucleon structure functions, νW_2^p, W_1^p, νW_2^n and W_1^n, presenting a mixed situation on the question of scaling. Among these form factors, some could be made to obey scaling either in ω or ω' or in a newly defined scaling variable which in the very deep scattering region approaches ω; others appear to manifest scaling breakdown. Also, not too surprisingly, differences exist in scaling behavior between proton and neutron structure functions. Up until now, similar experiments at FERMILAB have been and are being carried out only with muons[2] where the muon beam intensity is limited by design considerations to the level of 10^6 μ/pulse. As a result, the use of 20 feet long Fe targets is planned in order to obtain data at higher Q^2 values. Since, there seem to be unresolved differences between the scaling behavior of proton and neutron structure functions, Fe target experiments could hardly be expected to elucidate this important question. Of course, 30 feet long hydrogen and deuterium targets could be used for this purpose with muons, but the resulting sensitivity would be less than of this experiment.

Our experiment is based on the use of 24" long hydrogen and deuterium targets together with an electron/positron beam of 10^9 - 10^8 $e^{\pm}$/pulse. We therefore emphasize the need for exploring the lepton-nucleon deep inelastic scattering process with electrons at FERMILAB. Moreover, the long-standing electron-muon puzzle

and the possibility of observing anomalous leptonic behavior are of fundamental interest today, supporting the need for studying, at the same accelerator facility, both electron and muon induced scattering processes. In this case, different beam qualities and different detectors are involved, so that the relative comparisons of results will be sharp and clear.

III. ELECTRON BEAM

Compared with other lepton beams, electrons have an experimental advantage. A good quality electron beam is obtained in a relatively short beam line, delivering a small and clean beam spot at the experimental target. The high intensity Proton-West pion[3] beam will produce at no additional cost such a high intensity good quality electron[4] beam. This conversion is accomplished in a very simple way and is designated in Figure 2. Basically, a radiator is inserted and the beam line is retuned[5] in a well-known manner. The retuning of magnets is based on compensation of electron energy loss due to synchrotron radiation as electrons traverse beam line superconducting magnets. Moreover, to further purify the electron beam, additional enhancement of synchrotron radiation is produced by introducing reverse bends in some clusters of dipoles, while beam line geometry is preserved. Thus,by design, electrons are transmitted on optical axis along the entire beam line while contaminating hadrons become

separated off optical axis. At appropriate focal points these contaminants are successively removed by aperture stops, collimators and slits.

The following statements are based on detailed ray-tracing Monte Carlo studies on the implemented Proton-West beam design,[3] with magnets tuned to optimize synchrotron radiation compensation and with appropriate beam stops in required positions. The electron beam at the E-192 target location (75 feet downstream of the E-258 target) will have the following properties:

• Useful electron beam acceptance relative to production target	36.8 μsterad - % (FW)
• Electron beam momentum uncertainty	$\Delta p/p = \pm 1.9\%$
• Horizontal angular divergence	$\Delta\theta = \pm 0.4$ mrad
• Vertical angular divergence	$\Delta\varphi = \pm 0.3$ mrad
• Horizontal spot size	$\Delta x = \pm 3$ mm
• Vertical spot size	$\Delta y = \pm 4$ mm
• Hadronic contamination in electron beam	$\pi/e < 3 \times 10^{-6}$

The useful acceptance of the Proton-West beam line is 7 times larger than the acceptance of the Proton-East beam. Electron beam yield energy distributions are obtained by comparing electron yield calculations with measurements of electron beam intensities which were carried out by the E-25 collaboration at the Proton-East tagged photon beam area. These were made with 300 GeV incident protons. Renormalizing calculations by an arbitrary scale factor to match these over all the measured points and multiplying by the acceptance ratio of 7 , the electron yield curve shown in Figure 2

is obtained for $E_{proton} = 300$ GeV. Similarly, the electron beam yield curves for $E_{proton} = 400$ GeV and $E_{proton} = 500$ GeV follow from the established procedures. Therefore, the desired electron beam intensities upon which this experiment is based are obtained by running at proton energies somewhere between 400 GeV and 480 GeV, with 10^{13} incident protons/pulse on a 16" long Be target at 360 pulses/hour. We note that the targeting area of the Proton-West beam is being hardened to absorb 10^{14} incident protons/pulse and recent performance of the Batavia accelerator speaks emminently well for this achievement.

As shown in Figure 2, electrons are produced at the 1/8" Pb radiator with transverse momenta of $< p_{\perp}^{e} > = 8$ MeV/c caused by multiple scattering in the radiator. Background pions are produced by neutrons striking the radiator with transverse momenta of $< p_{\perp}^{\pi} > = 325$ MeV/c . Therefore, projecting back to the 16" Be target, the pion spot is 41 times larger than the electron spot. The electron source spot is essentially defined by the incident proton spot and is $\pm$ 1 mm . Immediately behind the Pb radiator the π/e ratio in the beam is 10^{-3} . Because of the large difference in source spot size between electrons and background pions, vertical slits at intermediate vertical foci remove 95 percent of the remaining pions. Due to the synchrotron radiation enhancement tuning, electrons travelling the entire beam line lose 3.6% of their energy while remaining on optical axis. Pions are transmitted with momenta between - 6.7% and + 2.3%

of the initial beam momentum tune and fall off optical axis at intermediate horizontal foci. At the first horizontal focus the pion spot centroid is shifted to the left by 8.5 mm, and because of cross-over optics, at the second horizontal focus, the spot centroid of surviving pions is shifted to the right also by 8.5 mm. There are very few unfortunate pions that manage to place themselves inside the electron beam spot and we set a figure of $\pi/e < 3 \times 10^{-6}$ at the E-192 target location. As will be shown in Section VII the background produced by these pions is less than the self-generated background produced by electrons.

Positron beam qualities are identical to the above stated electron beam qualities. This is the only installation we know of at very high energies, where electron and positron beams are made available under identical experimental conditions to an experimental apparatus. This desirable feature is extremely useful to the proposed e^--p and e^+- p deep inelastic scattering difference measurement.

IV. EXPERIMENTAL ARRANGEMENT AND GEOMETRIC ACCEPTANCE

We propose to use the experimental apparatus of E-192 with small additions and a minor repositioning , which is designed to intercept scattered electrons over a large range in Q^2 and W^2 together with optimum acceptance at the highest available Q^2 values. The scaled plan view of the experimental arrangement of E-192 is shown in Figure 3(a).

Essentially, the E-192 set-up is a large acceptance and large angle particle-pair spectrometer for the detection of $e/\mu/\gamma$ pairs in possible combinations. A smaller aperture first magnet is run in opposite polarity

with respect to a following magnet of a larger aperture, producing an achromatic focus on beam axis, behind the NaI spectrometer assemblies. All target-associated charged particles produced within a 50 mrad cone are focussed and the spectrometer arms are shielded from a large hadronic background.[6] Tracking information is obtained by MWPC's designated by 1 - 12 on this figure. Chambers 6,7,8 provide x,u,v coordinate information with wires oriented at 90°, 60° and 120° while the remaining chambers provide x,y coordinate information. Some of these chambers are tilted by $\pm 30^{\circ}$ with respect to others. Chambers 1 - 8 have successively increasing desensitized central zones for the unrecorded passage of beam tracks. Desired particles $e/\mu/\gamma$ produced at large angles are intercepted by spectrometer arms shown in detail in Figure 3(b).

Each spectrometer arm is composed of segments of 30" diameter NaI crystals followed by Pb and Fe absorbers. MWPC's with delay-line readout are placed between the front NaI segments and the absorbers in order to measure particle coordinate, intercepted shower multiplicity and pulse width above desired threshold levels. Up to four such particles entering a spectrometer arm can be recorded with particle-pair space resolution of 1". Chambers 1,2,3 of this arrangement are set at moderately high threshold, recording the large pulse heights of intercepted showers from electrons or gamma-rays. Chambers 4,5 are used predominantly for pion identification and chambers 6,7 provide muon identification. Pulse height from each NaI segment is recorded

and the sum signal is used to provide an energy acceptance in event triggers.

Single electrons or pions incident on a spectrometer arm can be easily identified by measuring the ratio of the total energy deposited in the NaI to the measured momentum obtained by track reconstruction from the magnet-MWPC system. The FWHM energy resolution of incident electrons and gamma-rays obtained by the NaI segments has been determined to be $1.5\% \times (35/E)^{1/4}$ at FERMILAB, where E is in units of GeV. Further information from NaI segments gives an electron-pion separation of at least $10^5:1$, similar to the experience found[7] in E-288. Tracking information for gamma-rays is obtained exclusively by MWPC's 1,2,3 while muons proceed through all the Fe downstream of the NaI.

The proposed experimental arrangement to measure the inclusive electron-nucleon deep scattering cross sections is shown to scale in Figure 4. The arrangement is essentially the same as in E-192. The spectrometer arms I and II are repositioned at a slightly different orientation and a third NaI spectrometer arm is included without Fe absorbers. The presence of the third arm does not cause any interference with the operation of E-192. Moreover, the polarity of the first magnet is made to be the same as the polarity of the following magnet. We also propose to use the 24" long LH_2/LD_2 target of E-192 for this experiment. The effects on radiative corrections caused by this target are discussed in detail in Section VIII. It is concluded that in the worst cases, use of a 24" long LH_2 target would increase the correction factors by 26% relative to the use of a 12" long LH_2 target. This creates no special

problems. Therefore, the changeover between E-192 and the electron experiment can be accomplished in a quick and straightforward manner. This is important, because we are proposing to run this experiment and E-192 in interleaved periods of time.

The incident electron beam is deflected slightly by passing through the experimental magnets and is absorbed in a Faraday cup located 50 feet behind the second magnet. A Faraday cup will be used to measure precisely the incident electron flux.

The inclusion of the third NaI spectrometer arm is important. It increases by at least a factor of 2 the overall acceptance at the highest available Q^2 regions. It also increases by a factor of 3 to 4 the acceptance at the highest available W^2 region where also $\epsilon \simeq 0$ and ω' values are high, and it provides a smooth overlap in acceptance at intermediate Q^2 and W^2 regions. The geometrical acceptance of the apparatus is calculated by the Monte Carlo technique, by generating scattered electrons uniformly distributed within a Q^2 region of $0 - 200\ (GeV/c)^2$ and within a kinematically allowed ν region as outlined in Figures 5,6 and 7, for incident electron beam energies of 150, 175 and 250 GeV, respectively. These figures show the fraction of the events accepted by the total apparatus in each $Q^2 - \nu$ bin. In addition, the regions within which the individual detection efficiency is greater than 5% are outlined for each spectrometer arm. At each energy, most of the $Q^2 - \nu$ domain is covered by arm I and II, while the third arm more than doubles the counting rates at the crucial

regions of large Q^2 and large ω or ω'. We conclude that the geometric acceptance of our apparatus is competitive with the acceptance to be found in 20 feet long Fe target muon experiments.

The problem of reliable electron identification for events with more than one particle entering in any single arm of the apparatus is discussed in detail in Section VII. It is concluded that throughout the experiment there will be a systematic ambiguity in the identification of scattered electrons due to accompanying pions which leads to a small error. In the worst case this systematic error is at the level of 1% of all detected electrons. It is found that such events are smoothly distributed throughout the (Q^2,W^2) acceptance domain and moreover, this systematic uncertainty is by far the smallest of all other accountable uncertainties.

Finally, according to detailed background studies, a scattered electron and an accompanying $\pi^{\pm}$ are separated by less than 5" in a given arm in about 12% of the events. Thus, a possible modularization of the 30" in diameter NaI segments into modules of 5" × 5" which might be contemplated by others still results in a considerable fraction of two particle hits in one such module. Edge effects and shower leakage into neighboring modules become important corrections in that case, in contrast to the simplicity of the system described here. We conclude that our proposed geometry which does not involve modules is the best for the purpose of this experiment.

V. EXPERIMENTAL RESOLUTION

The superior power of this experiment, relative to other experiments with similar physics objectives, lies in the experimental resolution of the kinematical variables Q^2, ν, W^2 and ω or ω'.

An example of the experimental resolution in ν is displayed in Figure 8 for both the case where energy measurement of scattered electrons is determined by pulse height in the NaI spectrometer arm when no other accompanying particles are present, and also for the case where E_e' is measured by magnetic analysis. Electron identification is always obtained from the NaI. Examples of the experimental resolution in Q^2 are given in Figure 9. In the limiting case, ΔQ^2 in this experiment is dominated by the angular resolution for values of $Q^2 < 20\ (\mathrm{GeV}/c)^2$, in contrast to the 20 feet long Fe-target muon experiments, in which ΔQ^2 and $\Delta \omega^2$ are dominated by $\Delta E'$. Good resolution in Q^2 is extremely important because it allows for fine binning of data in ω', thereby permitting a meaningful evaluation of cross sections at very large ω' values. The resulting experimental resolution in ω' is demonstrated in Figure 10.

A very strong advantage of this experiment is the ability to measure the inclusive electron-nucleon scattering cross sections at extremely high ω' values with good resolution, where event rates are also high.

VI. EVENT RATES AND REQUESTED RUNNING TIME

The counting rates anticipated in this experiment for electron beam bombardment on a 24" long LH_2 target are shown in (Q^2, W^2) bins in Figure 11, 12 and 13 at E_o = 150 GeV, 175 GeV and 250 GeV, respectively. These numbers are obtained from a Monte Carlo program which generated

scattered electrons according to the SLAC-MIT determined cross sections[1] for the inclusive deep inelastic electron-proton scattering. The numbers for electron bombardment on a 24" long LD_2 target increase by a factor of 1.7 .

The anticipated integrated total event counts at different Q^2 regions are summarized by the following:

450 HOURS ELECTRON BOMBARDMENT ON 24" LH_2 TARGET

Range of Q^2 $(GeV/c)^2$	75 hours @ E_o = 150 GeV	125 hours @ E_o = 175 GeV	250 hours @ E_o = 250 GeV
0 - 1	1.04×10^7	9×10^6	3.6×10^6
1 - 10	422,000	345,500	132,800
10 - 60	70,400	59,800	21,900
60 - 200	1,270	2,320	2,320

We also propose to run a total of 300 hours with positron beam bombardment on hydrogen, distributed as 50 hours at E_{e^+} = 150 GeV, 75 hours at E_{e^+} = 175 GeV and 125 hours at E_{e^+} = 250 GeV . The main purpose of a positron beam run is to study any two-photon exchange effects, which may have a profound influence in the determination of nucleon structure functions νW_2 and W_1 within an entirely unexplored (Q^2, W^2) domain. These effects manifest themselves in the difference of $e^+ - p$ and $e^- - p$ deep inelastic scattering cross sections, and we propose to measure the asymmetry

$$A(Q^2) = \frac{\sigma(e^+p) - \sigma(e^-p)}{\sigma(e^+p) - \sigma(e^-p)}$$ as a function of

Q^2 in the range of $Q^2 = 1 - 160\ (GeV/c)^2$. Of course, this investigation will also reveal if there exists any anomalous behavior in $A(Q^2)$ due to new physics at extreme Q^2 values.

The ability to separate the scattered electrons from other background electrons is crucial, since it is from the inclusive electron scattering cross sections that the behavior of nucleon form factors is extracted. The known effects of these backgrounds are discussed in Section VII. Another powerful feature of this experiment described in Section VII is the fact that a built-in self-calibration scheme is provided whereby all harmful background is subtracted by straightforward experimental calibration runs. For this purpose we request additional beam time, amounting 25% of the duration of normal data acquisition runs.

SUMMARY OF REQUESTED RUNNING TIME

At	E_o = 150 GeV	E_o = 175 GeV	E_o = 250 GeV	Total Hours
electrons on hydrogen	75 hours	125 hours	250 hours	450
electrons on deuterium	75 hours	125 hours	250 hours	450
positrons on hydrogen	50 hours	75 hours	175 hours	300
experimental calibrations	50 hours	80 hours	170 hours	300
				1,500

VII. BACKGROUND AND BACKGROUND RATES

We demonstrate that there are no background problems associated with our apparatus in this experiment and there are no rate limitations.

There are three types of background anticipated in this experiment where scattered electrons could be misidentified. We have made detailed Monte Carlo studies on the sources and effects of these types of background and conclude that there are no particular problems in obtaining measurements of deep inelastic electron scattering cross sections by our apparatus to within a limiting systematic uncertainty of a few percent. Other non-target-associated room background will not impair our measurements. These NaI assemblies have been shown to withstand a several MHz counting rate with no harmful signal degradation in a test especially performed for this purpose at FERMILAB.

One of the types of background is apparatus-associated where charged pions and electrons are accepted simultaneously in a given spectrometer arm. The second type of background is target-associated. This is a self-generated background of electrons due to the inclusive π^o electro-production process. The third type of background is beam-associated and is due to electron beam contaminant pions which are present at the level of beam $(\pi/e) < 3 \times 10^{-6}$. The latter two types can be described symbolically by the following chains:

Type II. $e^- \rightarrow e' + (\pi^o \rightarrow \gamma\gamma \rightarrow e_b^+ \; e_b^-)$ or $e^- \rightarrow e' + (\pi^o \rightarrow \gamma \; e_b^+ \; e_b^-)$

Type III. $\pi^- \rightarrow \pi^o \rightarrow \gamma\gamma \rightarrow e_b^+ \; e_b^-$ or $\pi^- \rightarrow \pi^o \rightarrow \gamma \; e_b^+ \; e_b^-$

where $e_b^{\pm}$ designates background electrons from pair-production or Dalitz decays and e' is used for real nucleon-scattered electrons. The average pair production rate in a 24" long LH_2 target is 2.6% per gamma-ray, while the Dalitz decay rate is 1.17%.

1. Particle Misidentification due to Electroproduced Charge Pions and Gamma Rays

We generated e-p inelastically scattered events containing electroproduced charged and neutral pions. In each event we generated multiple $\pi^{\pm}$ tracks based on a real statistical description as to their multiplicity, transverse momentum and longitudinal momentum obtained from recent measurements[2b] at FERMILAB in E-98. The reconstructed $\pi^{\pm}$ mean multiplicity was proportional to $1 + \ln W^2$ and averaged about 5 charged pions per event. In each event π^{o}'s were also generated using similar distributions based on a recently completed inclusive π^{o} electroproduction[8] experiment at SLAC. A single π^{o} was generated per event, as suggested by the preliminary data. Scattered electrons (e') were generated according to a uniform distribution within a range of $Q^2 = 0 - 200\ (GeV/c)^2$ and $W^2_{min} = 4\ GeV^2$ to W^2_{max} for each electron beam energy of interest, in order to detect any correlation between $\pi^{\pm}$e' or γ e' multiple hits in a given (Q^2, W^2) grid and a given spectrometer arm. An insignificant correlation between such hits at increasing W^2 was observed. Therefore, the results of this study are presented for the case of $E_o = 250$ GeV in Table I, averaged over the entire (Q^2, W^2) domain. The results for $E_o = 175$ GeV and 150 GeV are similar.

From Table I, we conclude that in this experiment a charged pion or a gamma-ray would accompany an accepted e' in about half of the events. In the e'γ category, the e' is readily identified from tracking information and very large pulse heights in the NaI segments and its energy is determined

TABLE I

MULTIPLE HITS IN SPECTROMETER ARMS DUE TO ELECTROPRODUCTION OF MULTIPLE $\pi^{\pm}$'s AND π^{o}, AT E_o = 250 GeV

	Arm I	Arm II	Arm III
percent e'γ prompt hits in spectrometer arm	5.3	1.8	< 0.1
$\langle E_\gamma \rangle$ in GeV for e'γ hits	12.3	11.3	-
$\langle E_{e'} \rangle$ in GeV for e'γ hits	90.9	78.7	-
percent of e'γ events with separation less than 2" at spectrometer arm	< 1.0	3.0	-
percent e'π prompt hits in spectrometer arm	44.2	34.5	30.1
$\langle E_\pi \rangle$ in GeV for e'π hits	30.9	31.4	15.8
$\langle E_{e'} \rangle$ in GeV for e'π hits	95.4	94.7	63.3
percent of e'π events with separation less than 2" at spectrometer arm	2.7	1.7	2.0

from magnetic analysis. In the e'π^- category there are two reconstructed charged tracks and the problem is one of assigning the correct track to the e'. In such cases, pulse height from the delay line readout MWPC's (1 - 5) located between NaI segments and behind Pb and Fe absorbers provide sufficiently redundant information to reduce the e'-π ambiguity to less than 0.5%. The $\pi^-\gamma$ case can be similarly distinguished from the e'γ category and be excluded. The worst situation occurs when in the e'π^- category the particle-pair at a spectrometer arm is separated by less than 2", so that the showers begin to overlap and tracking extrapolation may become marginal in separating the two particles. This happens less than 2% of the time (cf. Table I), so that the net effect is an ambiguity in about 1% of the e' triggered events, which is well within the statistical and other systematic uncertainties of this experiment.

2. Self-Generated Background Electrons from Beam Electrons (Type II Process).

The most serious background is due to real electrons, e_b, from type II and type III processes where the e_b cannot be distinguished from true inelastically scattered e' electrons. This is an inherently self-generated background which is present in all electron scattering experiments. The Monte Carlo program used to study these events generated scattered electrons (e') according to experimentally measured[1,2] distributions in Q^2 and W^2 and also generated π^o's according to the above mentioned procedure.

Table II summarizes the results of these studies at E_o = 150, 175 and 250 GeV where also the anticipated counting rate/pulse from all types of electron interactions is given. We see that there are no counting rate limitation problems in this experiment.

The low fraction of e_b relative to e' is misleading because almost all background electrons (e_b) are found clustered at the highest W^2 region near the kinematical boundary, with Q^2 values below 20 $(GeV/c)^2$. In the highest W^2 bin the e_b rate exceeds the e' rate for Q^2 values of less than a few $(GeV/c)^2$. In 40% of the e_b rates the e' is also detected, half the time in the same spectrometer arm, but there is no reliable way of distinguishing one from the other.

TABLE II

BACKGROUND ELECTRON RATES FROM ELECTRON BEAM INTERACTIONS IN 24" LONG LH_2 TARGET

(Entries are given in percent of accepted scattered electrons)

Electron Beam	150 GeV	175 GeV	250 GeV
1 e_b^-, without e' accepted	0.38	0.75	1.29
2 e_b^-, without e' accepted	0.0005	0.001	0.004
1 e_b^-, with e'	0.55	0.63	0.86
1 e_b^-, with e' in same spectrometer arm	0.24	0.30	0.46
2 e_b^-, with e'	0.001	0.002	0.003
$e_b^+ + e_b^-$ with (e' or e_b^-) in two detectors	0.17	0.18	0.33
$e_b^+ + e_b^-$ in same spectrometer arm	less than 0.05% of all e_b		
COUNTING RATES/PULSE			
e^-	385	200	40
$\pi^\pm$	550	375	95
γ	315	280	70

Fortunately, there exists a well-known experimental calibration technique described below in subsection 4, which is used in all good precision electron scattering experiments. This technique corrects for this background up to the highest W^2 bin and for Q^2 values of more than a few $(GeV/c)^2$. Below such values of Q^2 and at the highest W^2 bins for a given beam energy, the e_b background rate is too copious to permit meaningful calibration measurements and, not too surprisingly, this is also the (Q^2,W^2) region where the radiative corrections are large. Therefore, this very restricted region at each given beam energy is avoided.

3. Background Electrons from Beam Contaminated Pions (Type III Process).

The hadronic contamination in the electron beam is mostly composed of π^-'s at the level of $\pi/e < 3 \times 10^{-6}$. These pions will produce π^o's with mean multiplicity of 3.5, from which pair-produced electrons and Dalitz decay electrons will appear in the apparatus. The Monte Carlo program used earlier[6] was modified to account for the differences between E-192 and this experiment based on differences seen in Figure 3(a) and 4.

The important conclusion of this precise study is that background electrons (e_b) obtained from the Type III process will cluster in the highest W^2 and low Q^2 region, moreso than the e_b produced by electrons from the Type II process. The e_b counting rates, based

on pion contamination of 3×10^{-6}, are less than the e_b rates from beam electrons, as can be seen in Table III. This table also summarizes the expected counting rates per pulse induced by beam contaminating pions. The calibration for this background is automatically performed during the calibration for the electron beam generated background, which must be carried out in any electron scattering experiment. Thus, a potential $\pi/e = 3 \times 10^{-6}$ contamination in the FERMILAB electron beam has no effect on the quality of this experiment.

To complete this section we note that the high π^o multiplicity in pion beam induced interactions allows the effective mass of a detected e_b^+, e_b^- coincidence to be as large as 2.5 GeV. However, the Monte Carlo study indicates that there would be fewer than <u>two</u> e_b^+, e_b^- events with effective mass between 2.0 and 2.5 GeV and none with higher mass in the entire $E_o = 250$ GeV proposed run. This number is reduced at $E_o = 150$ or 175 GeV, so that there is little background associated with the observation of any high mass dielectrons produced by electrons. Background dielectron masses due to the π^o electroproduction process, (e', e_b^+), are less than 0.5 GeV.

4. <u>Background Correction Procedure Via Calibration Run</u>

The last entry in Table II shows that no more than 0.05% of the e_b^+ produced by electron beam interactions are detected simultaneously with an e_b^- in the <u>same</u> spectrometer arm. This is also true of the $e_b^\pm$

TABLE III

BACKGROUND ELECTRON RATES FROM PION BEAM INTERACTIONS IN 24" LONG LH_2 TARGET

For $\pi/e = 3 \times 10^{-6}$

(Entries are given in percent of accepted scattered electrons)

Beam Energy	150 GeV	175 GeV	250 GeV
	%	%	%
1 e_b^- detected	0.46	0.59	0.84
2 e_b^- detected	0.22	0.32	0.52
3 e_b^- detected	0.002	0.003	0.005
e_b^+, e_b^- one in each spectrometer arm	0.004	0.007	0.010
$e_b^+ + e_b^-$ in same spectrometer arm	Less than 0.03% of all e_b^-		

COUNTING RATES/PULSE

e^-	.3	1	3
$\pi^\pm$	190	110	25
γ	100	70	15

background produced by contaminant pion beam interactions. These $e_b^{\pm}$'s are produced primarily in the forward direction (they have low apparent Q^2), and are not energetic (they have high apparent W^2), so that the e_b^+'s emerge from the magnetic field in the opposite side of the beam line from the e_b^-'s . Hence, the e_b^+'s strike only arm I and the e_b^-'s are absorbed by arms II and III, so that background positrons and background electrons are separated cleanly in the apparatus.

Reversing the field in both magnets will cause the opposite effect and counting e_b^+'s in this situation will indicate precisely the number of e_b^-'s to be subtracted in the normal mode of data acquisition. Therefore, our apparatus and experiment has a built-in self-calibration which is obtained by a straightforward experimental technique rather than some Monte Carlo type calculation. As an extreme example, if there were 1000 e' counts and 1000 e_b^- counts detected in a given (Q^2,W^2) bin, and a reverse field calibration run of 25% of the duration of the normal run were made, this subtraction technique would yield:

(2000 ± 45)	-	4	×	(250 ± 16)	=	1000 ± 77 events
events from normal field mode				events from reversed field mode		

or an 8% measurement in this case.

VIII. RADIATIVE CORRECTIONS

It is necessary to apply radiative corrections on data obtained from electron scattering and muon scattering experiments. These corrections are well understood and the technique[9] of their application is by now a straightforward matter. In deep inelastic electron-nucleon scattering all measured cross sections are corrected by a factor δ which is a function of beam electron energy E_o, scattered electron energy E' and scattering angle θ_e. An example case for $E_o = 175$ GeV and $\theta_e = 2.5^o$ is demonstrated in Figure 14 where terms defining the correction factor δ is also outlined. Using up-to-date radiative correction programs, the functional dependence of δ on W^2 is displayed. The equivalent dependence on ν or Q^2 is given. Shown are four separate curves.

The upper two curves are for μ-p and e-p scattering on zero target length, representing the amount of radiative corrections due to internal bremsstrahlung caused by the lepton-nucleon scattering process itself. The lower two curves are for e-p scattering on 12" long and 24" long LH_2 targets, showing the additional effect of straggling or external bremsstrahlung.

The last three curves show that the use of 24" long LH_2/LD_2 targets does not introduce any appreciable increase to the amount of radiative corrections, over that which is inherently present in electron scattering.

IX. EXPERIMENTAL SENSITIVITIES

The 3-point and adjacent 2-point separation regions in the (Q^2, W^2) domain to which this experiment is sensitive is shown in Figure 15, for the separation of structure functions νW_2 and W_1. The selection of these regions is based on the statistical accuracy in determining the inclusive cross sections as a function of E_o in a given (Q^2, W^2) bin, and on the values of the polarization parameter ϵ spanned by the three electron beam energies. It is demonstrated that the background and radiative corrections become severe only at the highest W^2 bin at a given energy and for Q^2 values of less than a few $(GeV/c)^2$.

In this experiment these separation regions permit the study of the nucleon inelastic form factors over a large Q^2 range of 0.16 - 100.0 $(GeV/c)^2$ and also over an ω' range of 1 - 100 or more. Moreover, this range will be studied with a fine resolution which is unattained in μ-Fe scattering experiments. In comparison, experiments at SLAC have directly measured the behavior of nucleon structure functions up to a Q^2 of 20 $(GeV/c)^2$ and for ω' values of up to 8. SLAC results presented at higher ω' values are extrapolations from a <u>guess</u> as to what the Q^2 "turn on" behavior at high ω' should be. The expected results shown for this experiment will be based on <u>direct</u> measurements up to values of $\omega' = 100$ or more for the separation and study of behavior of νW_2 and W_1.

Finally, any deviations from scaling behavior of electron scattering cross sections at increasing Q^2 will be investigated with experimental sensitivity illustrated in Figure 16. The points in this figure are the anticipated results from a total of 450 hours of data acquisition distributed over the three beam energies. Error bars include statistical errors and systematic uncertainties due to beam flux monitoring, radiative corrections and calibrated background subtractions.

X. SCOPE OF THE EXPERIMENT

Since results from on-going muon scattering experiments at FERMILAB are known and the scope of other planned muon beam experiments is also known, we stress that this electron experiment is even more important today than when it was originally conceived and proposed.

We emphasize that our FERMILAB pion experiment E-192 at the Proton-West Experimental Hall and the electron experiment outlined in this proposal are intimately connected. The relation exists not only in the commonality of beam line, apparatus and other experimental facilities, but also most importantly in the physics, as we plan to probe via respective experiments the time-like and space-like Q^2 regions at the highest available Q^2 values. In both cases these experiments will be examining kinematical regions which are unexplored up to the present time.

We wish to run both experiments in an interleaved way and make quick, efficient comparisons of results. A good example of what we mean is the case of experiments E-87A and E-358 where broad-band photon and neutron beams were used. It is by a similarly efficient comparison of results from complementary experimental runs that we expect to acquire new knowledge on the main features of the nucleon constituents.

Finally, we emphasize that during measurement of the inclusive deep inelastic electron scattering cross sections, our apparatus will observe and concurrently measure the following particle-pair inclusive reactions:

(a) $e\,N \rightarrow e^{-}\gamma + \text{anything}$

(b) $e\,N \rightarrow e^{-}\pi^{o} + \text{anything}$

(c) $e\,N \rightarrow e^{-}\mu^{\pm} + \text{anything}$

(d) $e\,N \rightarrow e^{-}h^{\pm} + \text{anything}$

(e) $e\,N \rightarrow e^{-}e^{\pm} + \text{anything}$

(f) $e\,N \rightarrow \mu^{-}\mu^{+} + \text{anything}$

(g) $e\,N \rightarrow \gamma\,\gamma + \text{anything}$

Reactions (a) - (e) will be found in the inclusive electron scattering master triggers while triggers for (f) and (g) are a simple extension of the general event triggering scheme. There are no event rate, data rate, or background rate limitations in the observation of these reactions as demonstrated in Sections VI and VII. It is the desirable nature of an electron beam experiment at FERMILAB and the apparatus of E-192 which make possible the concurrent observation of these exciting reaction channels. For example, anomalous leptonic production events similar to reaction (c) have been observed[10] at SPEAR at the level of branching ratio times cross section $B \cdot \sigma = 2 \times 10^{-35}$ cm^2. Our experimental luminosity at $E_e = 150$ GeV on 24" long LH_2 target is 5×10^{35} cm^{-2}/hour. We estimate an average detection efficiency of 10% for the observation of such events in our apparatus for $M_{e\mu}$ mass in the range of 2 GeV to 8 GeV. Typically, therefore, our experimental sensitivity for collecting 100 events in 100 hours of running is:

$$B \cdot \sigma = \frac{100 \text{ events}}{100 \text{ hours} \times (0.10) \times 5 \times 10^{35} \text{cm}^{-2}/\text{hour}} = 2 \times 10^{-35} \text{ cm}^2 ;$$

while experimental limiting sensitivity if no such events are observed is at the level of $B \cdot \sigma = 10^{-37}$ cm^2.

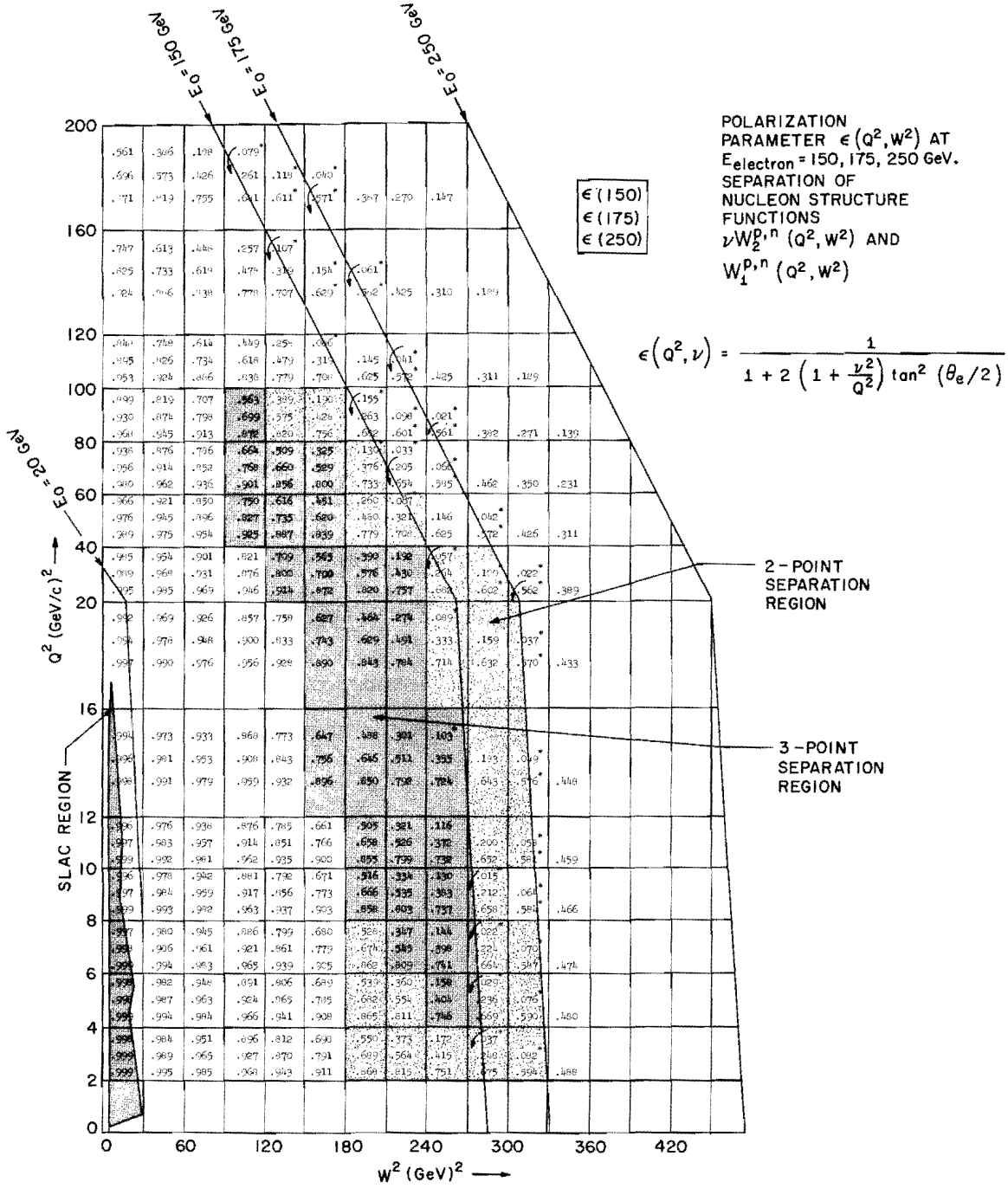
E0 = 150 GeV
E0 = 175 GeV
E0 = 250 GeV
E0 = 20 GeV
ϵ(150)
ϵ(175)
ϵ(250)
POLARIZATION PARAMETER $\epsilon(Q^2, W^2)$ AT $E_{electron}$ = 150, 175, 250 GeV.
SEPARATION OF NUCLEON STRUCTURE FUNCTIONS $\nu W_2^{p,n}(Q^2, W^2)$ AND $W_1^{p,n}(Q^2, W^2)$
$\epsilon(Q^2, \nu) = \frac{1}{1 + 2\left(1 + \frac{\nu^2}{Q^2}\right)\tan^2(\theta_e/2)}$
2-POINT SEPARATION REGION
3-POINT SEPARATION REGION
SLAC REGION
Q^2 (GeV/c)^2
W^2 (GeV)^2
0
60
120
180
240
300
360
420
0
2
4
6
8
10
12
16
20
40
60
80
100
120
160
200

FIGURE 1

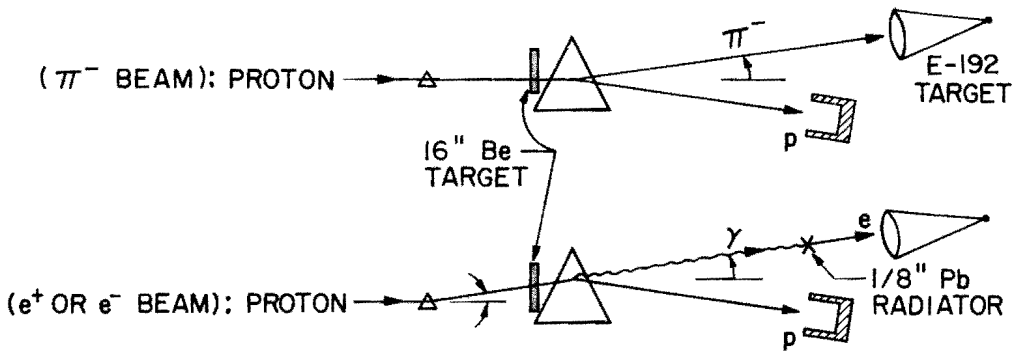

PROTON - WEST SUPERCONDUCTING BEAM LINE
ACCEPTANCE: 36.8 μsterad - % (FW)

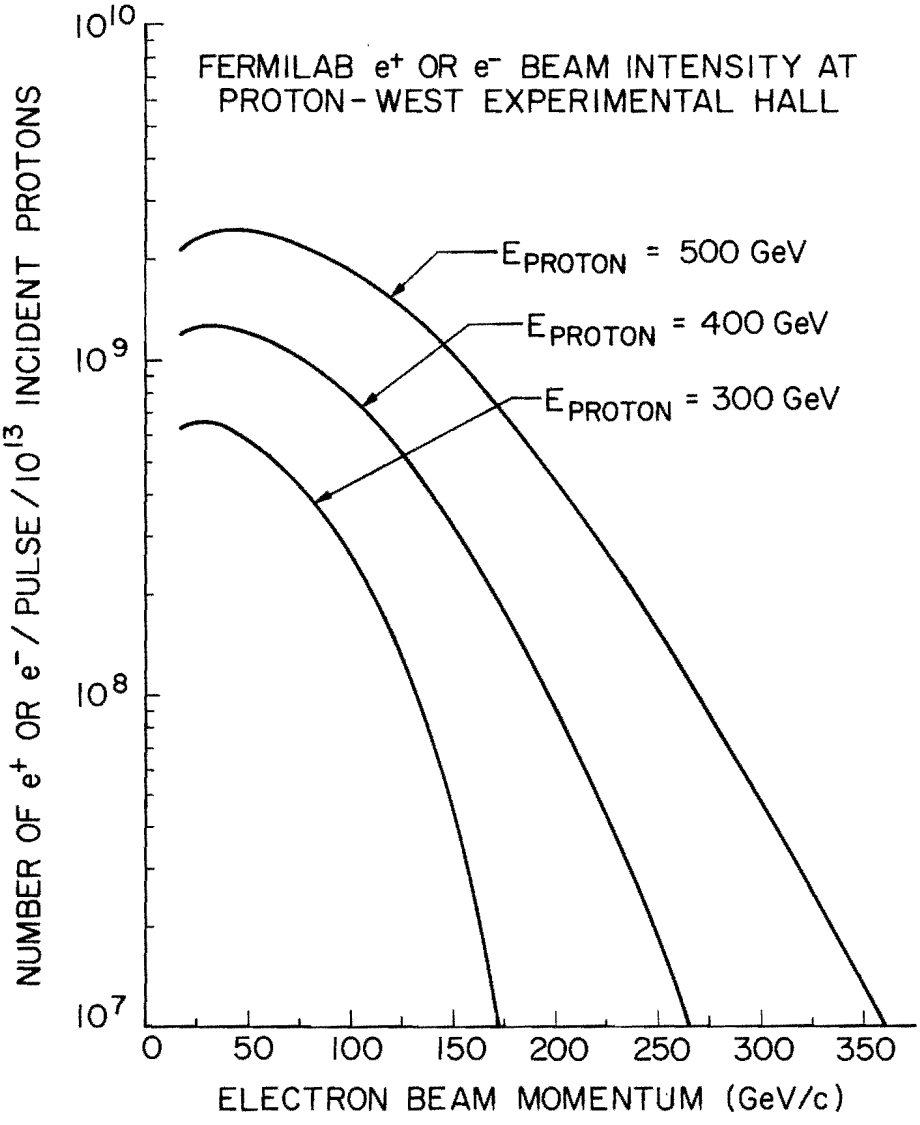

FIGURE 2

FERMILAB EXPERIMENT E-192, PROTON-WEST EXPERIMENTAL HALL

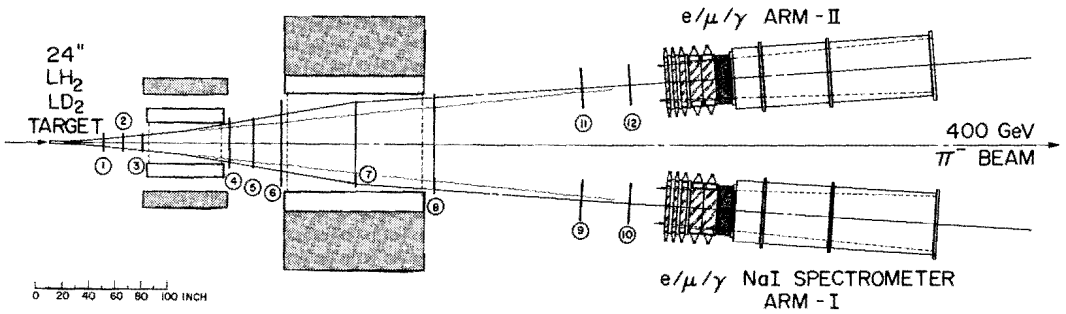

FIGURE 3 (a)

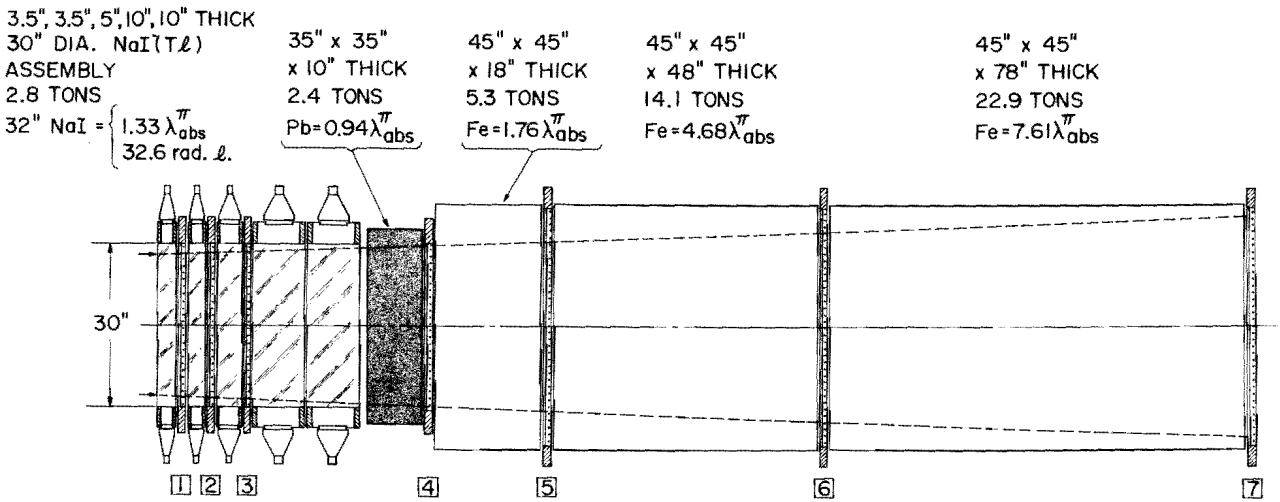

SPECTROMETER ARM FOR ELECTRON/GAMMA-RAY/MUON/HADRON DETECTION

FIGURE 3 (b)

FERMILAB ELECTRON-NUCLEON DEEP INELASTIC SCATTERING EXPERIMENT
PROTON-WEST EXPERIMENTAL HALL

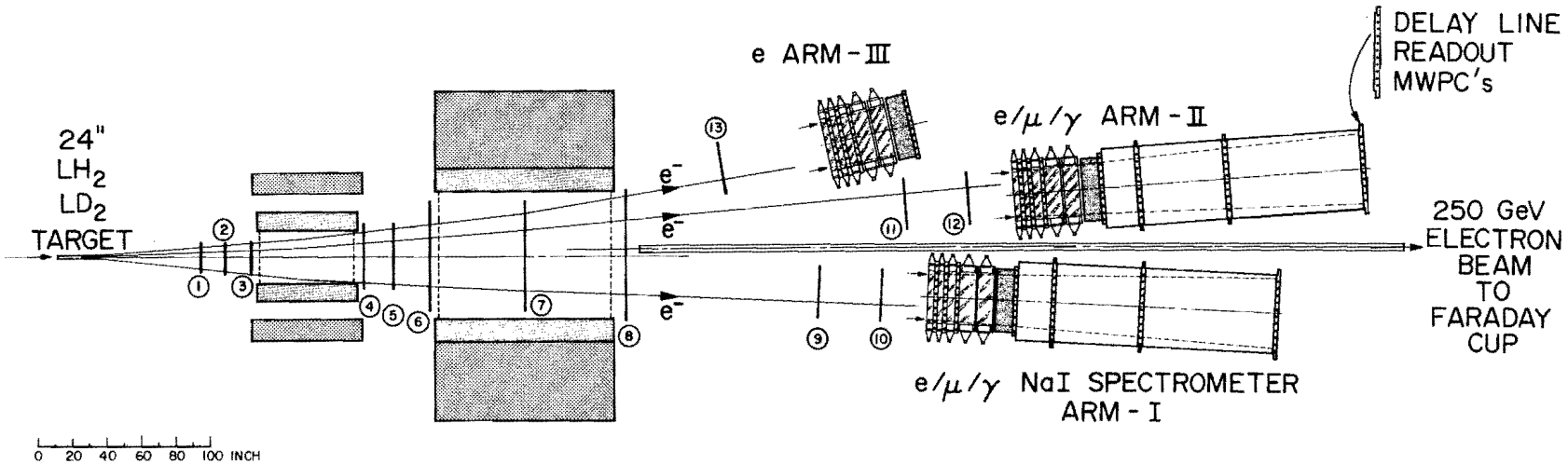

FIGURE 4

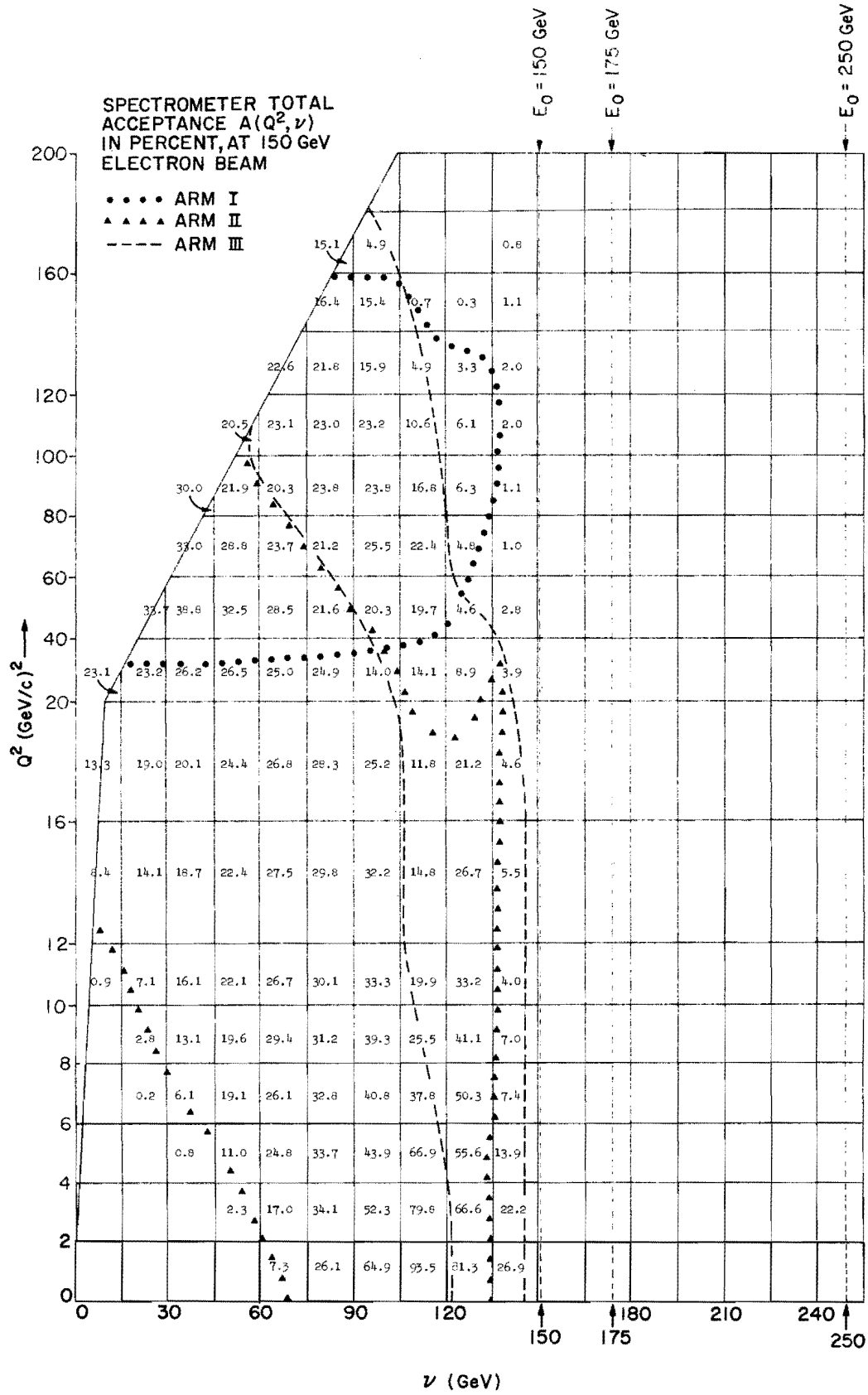
SPECTROMETER TOTAL ACCEPTANCE A(Q², ν) IN PERCENT, AT 150 GeV ELECTRON BEAM
ARM I
ARM II
ARM III
E0 = 150 GeV
E0 = 175 GeV
E0 = 250 GeV
Q² (GeV/c)²
ν (GeV)
0
30
60
90
120
150
180
210
240
175
250
2
4
6
8
10
12
16
20
40
60
80
100
120
160
200

FIGURE 5

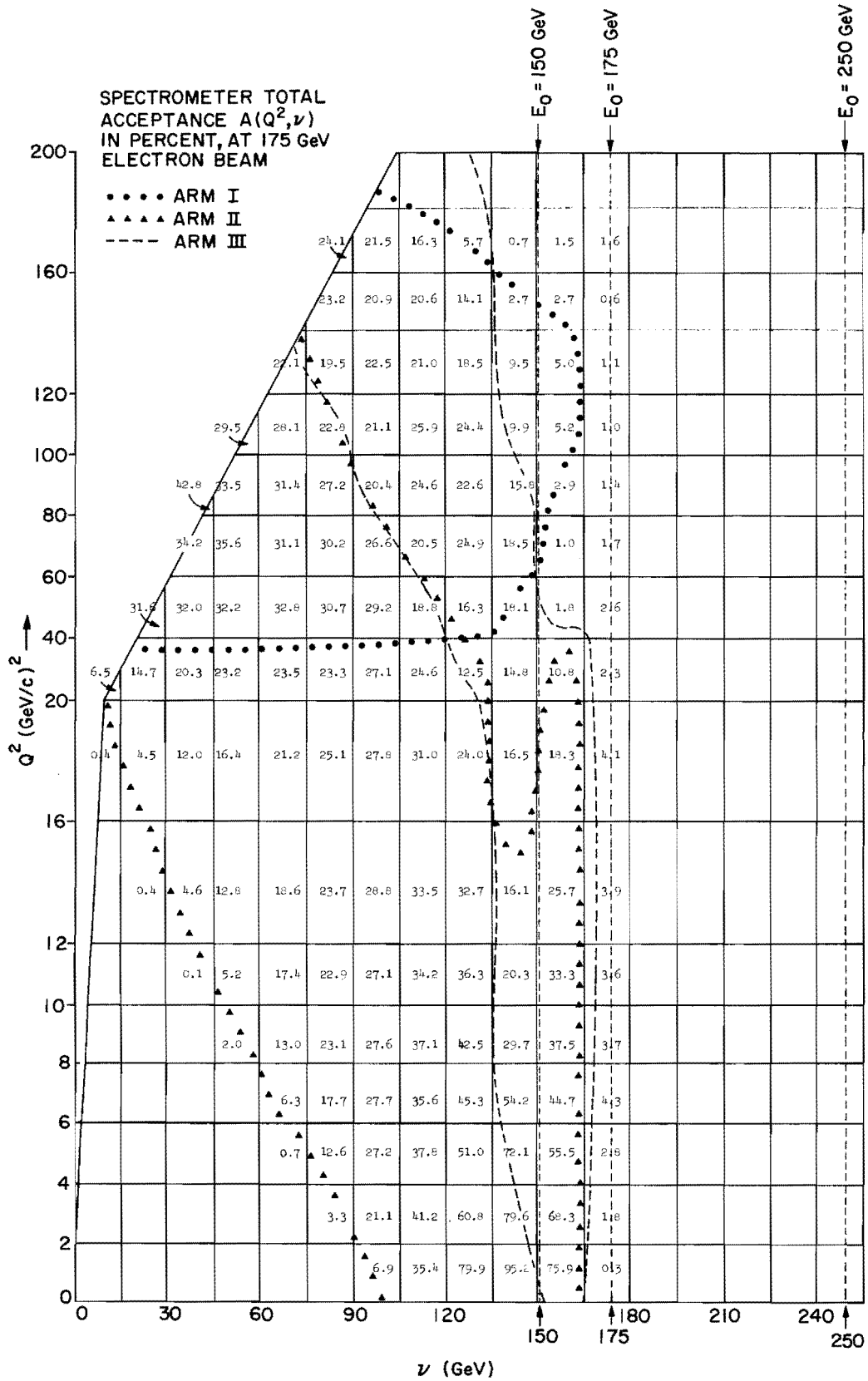
SPECTROMETER TOTAL ACCEPTANCE A(Q², ν) IN PERCENT, AT 175 GeV ELECTRON BEAM
ARM I
ARM II
ARM III
E₀ = 150 GeV
E₀ = 175 GeV
E₀ = 250 GeV
Q² (GeV/c)²
ν (GeV)
0
30
60
90
120
150
175
180
210
240
250
200
160
120
100
80
60
40
20
16
12
10
8
6
4
2
0

FIGURE 6

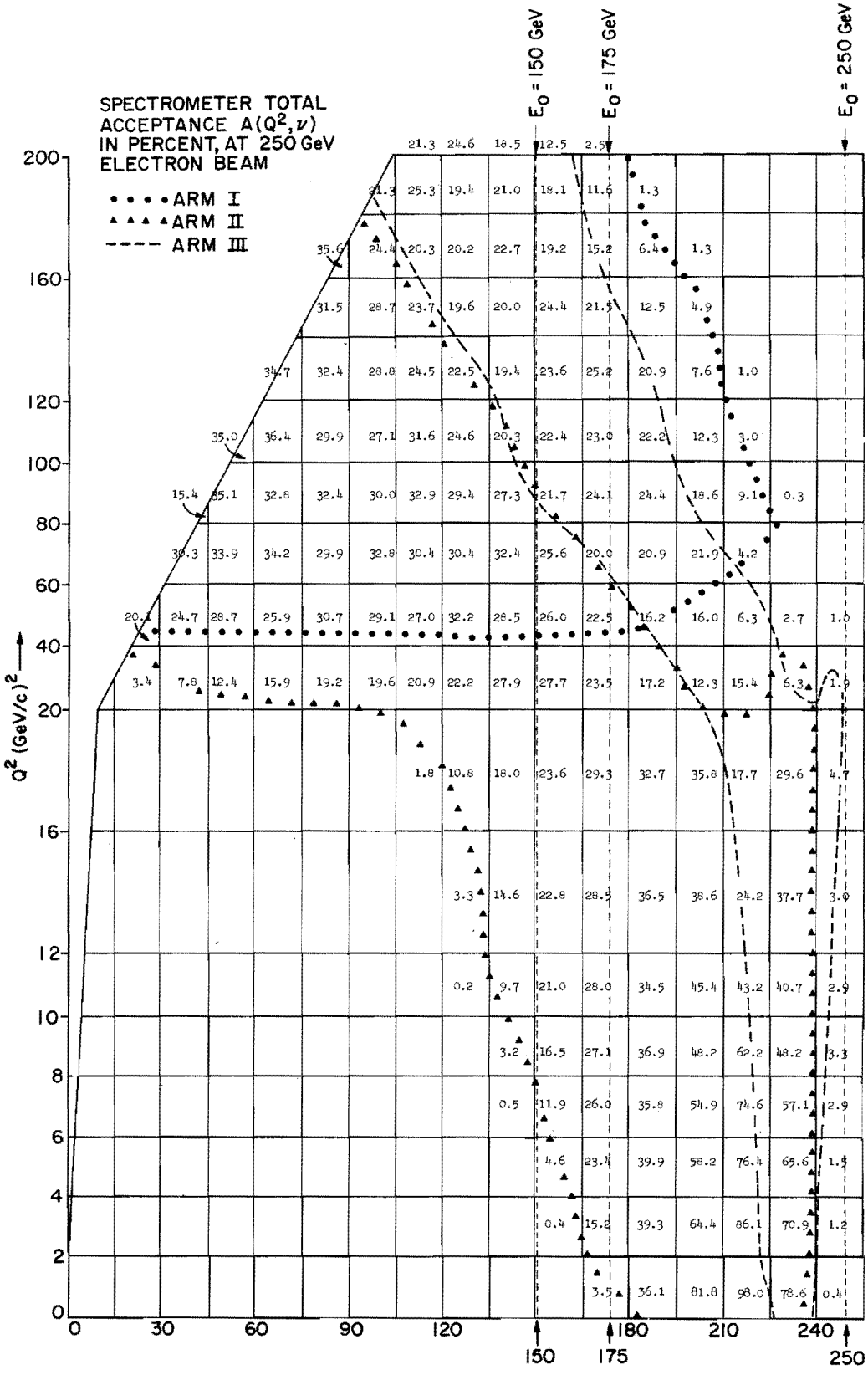
SPECTROMETER TOTAL ACCEPTANCE A(Q², ν) IN PERCENT, AT 250 GeV ELECTRON BEAM
ARM I
ARM II
ARM III
E₀ = 150 GeV
E₀ = 175 GeV
E₀ = 250 GeV
Q² (GeV/c)²
ν (GeV)
0
30
60
90
120
150
175
180
210
240
250
2
4
6
8
10
12
16
20
40
60
80
100
120
160
200

FIGURE 7

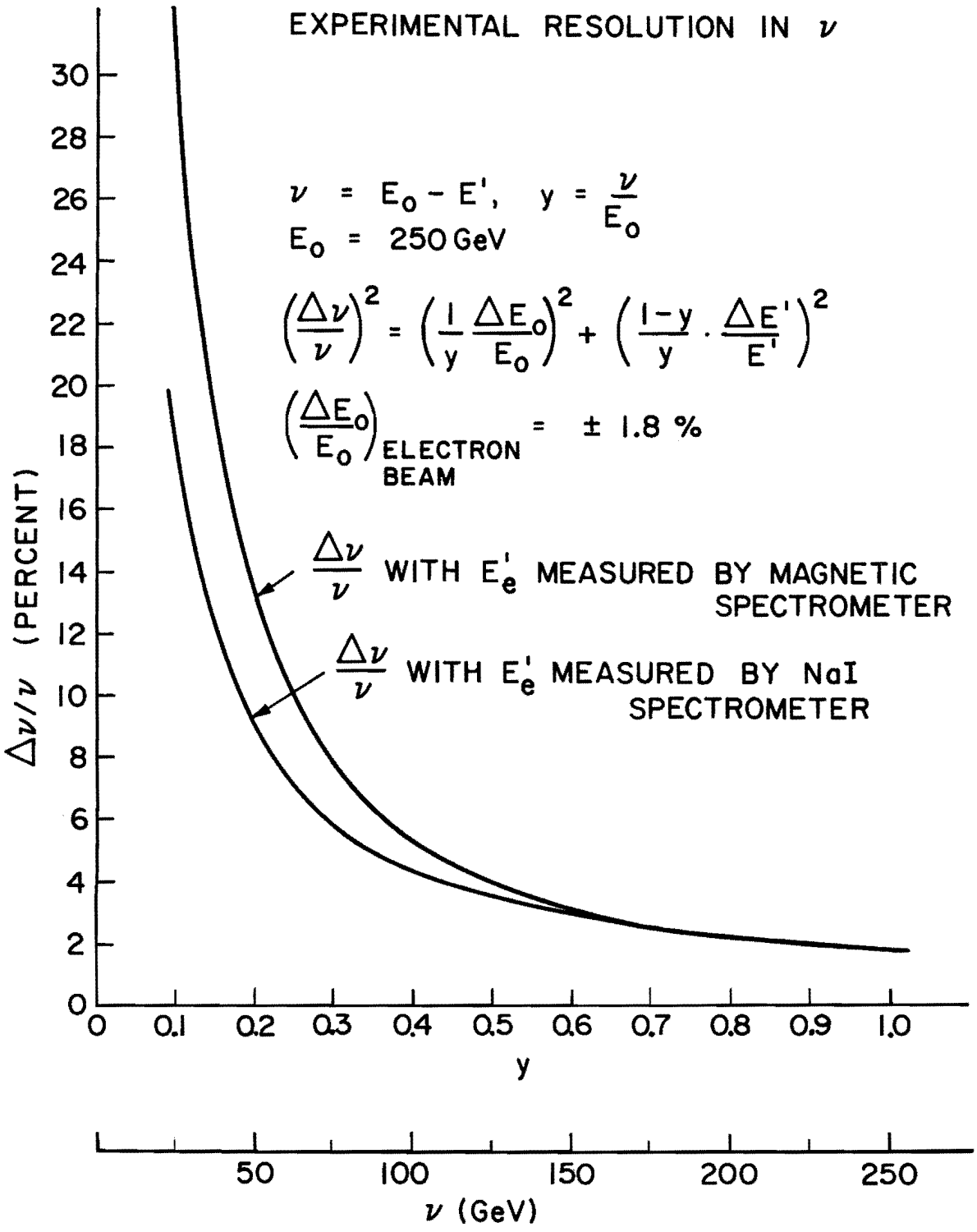
EXPERIMENTAL RESOLUTION IN ν
$\nu = E_0 - E'$, $y = \frac{\nu}{E_0}$
$E_0 = 250\,GeV$
$\left(\frac{\Delta\nu}{\nu}\right)^2 = \left(\frac{1}{y}\frac{\Delta E_0}{E_0}\right)^2 + \left(\frac{1-y}{y}\cdot\frac{\Delta E'}{E'}\right)^2$
$\left(\frac{\Delta E_0}{E_0}\right)_{ELECTRON\ BEAM} = \pm 1.8\ \%$
$\frac{\Delta\nu}{\nu}$ WITH E'_e MEASURED BY MAGNETIC SPECTROMETER
$\frac{\Delta\nu}{\nu}$ WITH E'_e MEASURED BY NaI SPECTROMETER
$\Delta\nu/\nu$ (PERCENT)
0 2 4 6 8 10 12 14 16 18 20 22 24 26 28 30
0 0.1 0.2 0.3 0.4 0.5 0.6 0.7 0.8 0.9 1.0
y
50 100 150 200 250
ν (GeV)

FIGURE 8

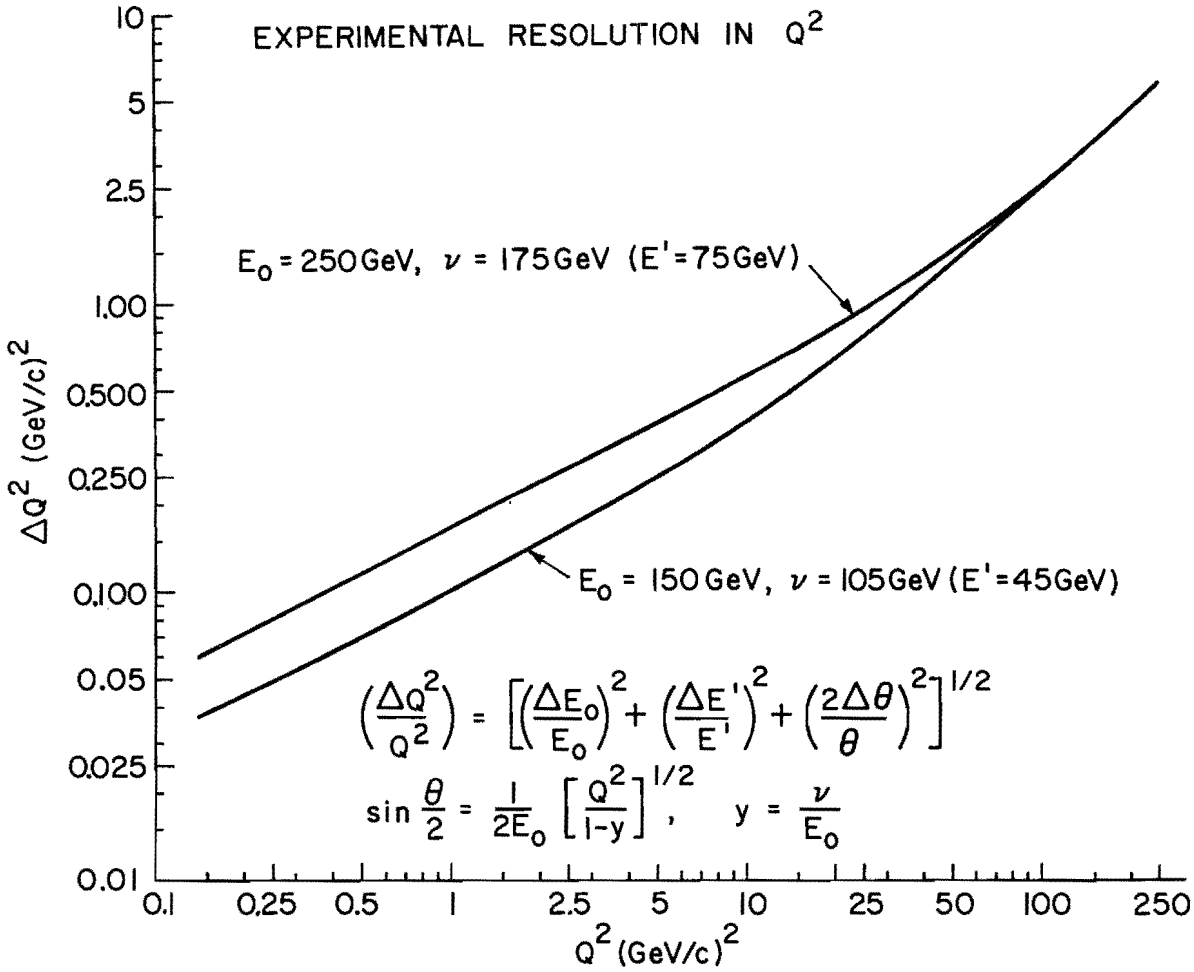
EXPERIMENTAL RESOLUTION IN Q^2
$E_0 = 250\,GeV,\ \nu = 175\,GeV\ (E' = 75\,GeV)$
$E_0 = 150\,GeV,\ \nu = 105\,GeV\ (E' = 45\,GeV)$
$\left(\frac{\Delta Q^2}{Q^2}\right) = \left[\left(\frac{\Delta E_0}{E_0}\right)^2 + \left(\frac{\Delta E'}{E'}\right)^2 + \left(\frac{2\Delta\theta}{\theta}\right)^2\right]^{1/2}$
$\sin\frac{\theta}{2} = \frac{1}{2E_0}\left[\frac{Q^2}{1-y}\right]^{1/2}, \quad y = \frac{\nu}{E_0}$
$\Delta Q^2\ (GeV/c)^2$
$Q^2\ (GeV/c)^2$
10
5
2.5
1.00
0.500
0.250
0.100
0.05
0.025
0.01
0.1
0.25
0.5
1
2.5
5
10
25
50
100
250

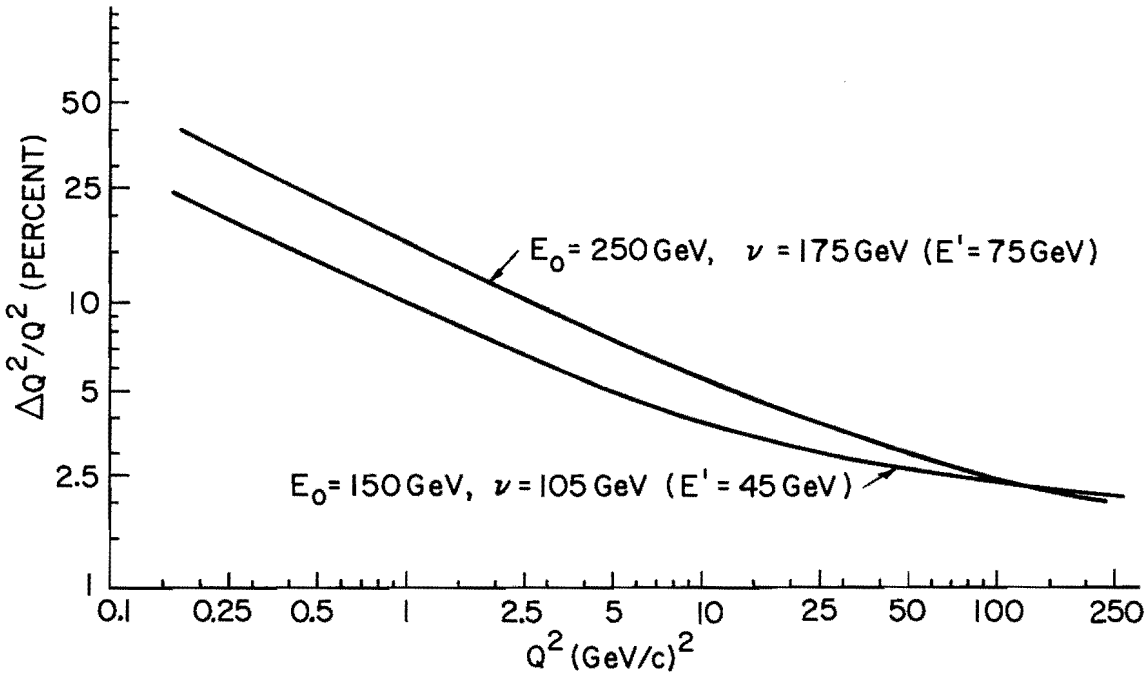
$E_0 = 250\,GeV,\ \nu = 175\,GeV\ (E' = 75\,GeV)$
$E_0 = 150\,GeV,\ \nu = 105\,GeV\ (E' = 45\,GeV)$
$\Delta Q^2/Q^2$ (PERCENT)
$Q^2\ (GeV/c)^2$
50
25
10
5
2.5
1
0.1
0.25
0.5
1
2.5
5
10
25
50
100
250

FIGURE 9

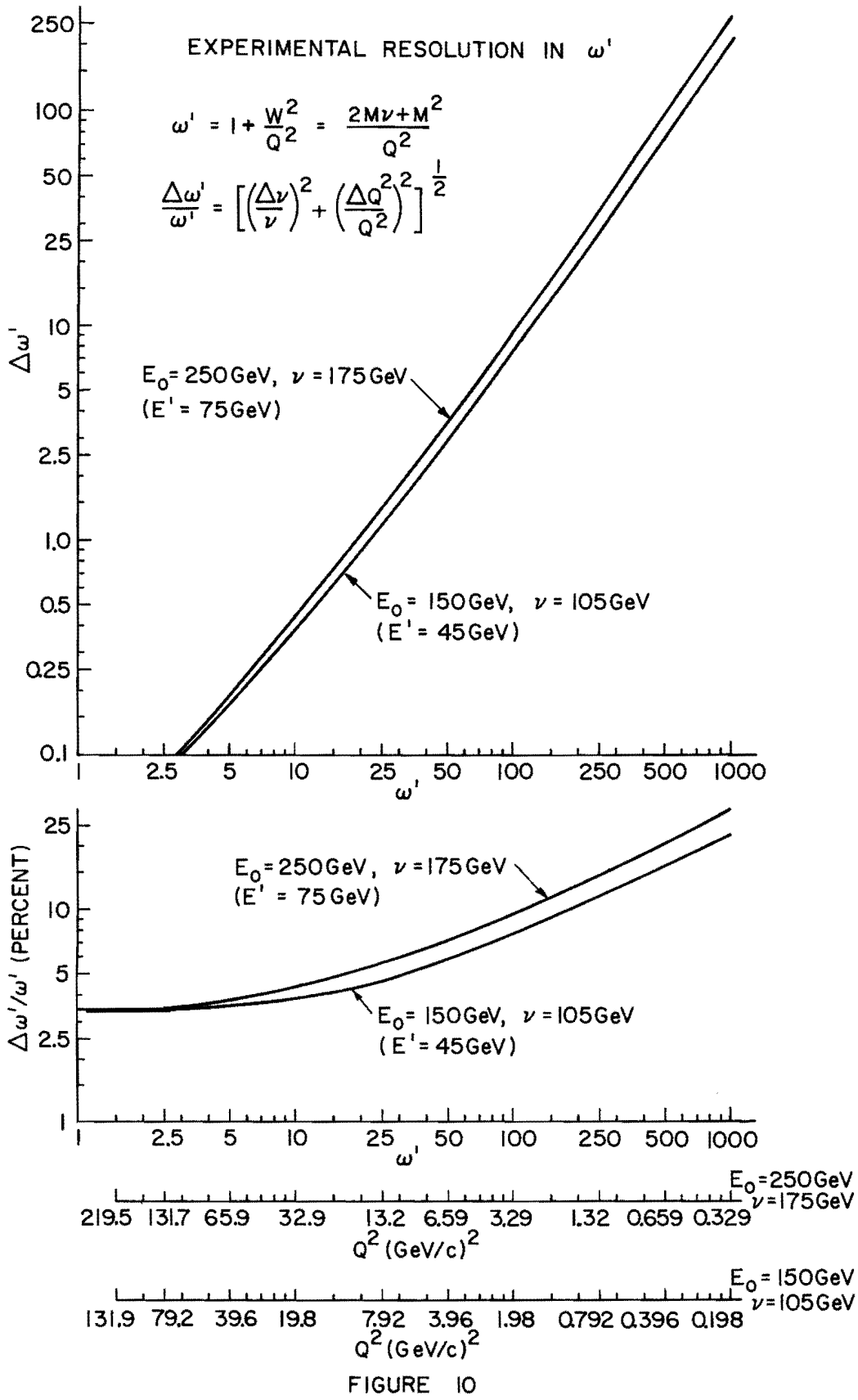
EXPERIMENTAL RESOLUTION IN ω'
$\omega' = 1 + \frac{W^2}{Q^2} = \frac{2M\nu + M^2}{Q^2}$
$\frac{\Delta\omega'}{\omega'} = \left[\left(\frac{\Delta\nu}{\nu}\right)^2 + \left(\frac{\Delta Q^2}{Q^2}\right)^2\right]^{\frac{1}{2}}$
Δω'
250
100
50
25
10
5
2.5
1.0
0.5
0.25
0.1
E0 = 250GeV, ν = 175GeV
(E' = 75GeV)
E0 = 150GeV, ν = 105GeV
(E' = 45GeV)
1
2.5
5
10
25
50
100
250
500
1000
ω'
Δω'/ω' (PERCENT)
25
10
5
2.5
1
E0 = 250GeV, ν = 175GeV
(E' = 75GeV)
E0 = 150GeV, ν = 105GeV
(E' = 45GeV)
ω'
E0 = 250GeV
ν = 175GeV
219.5 131.7 65.9 32.9 13.2 6.59 3.29 1.32 0.659 0.329
Q2 (GeV/c)2
E0 = 150GeV
ν = 105GeV
131.9 79.2 39.6 19.8 7.92 3.96 1.98 0.792 0.396 0.198
Q2 (GeV/c)2

FIGURE 10

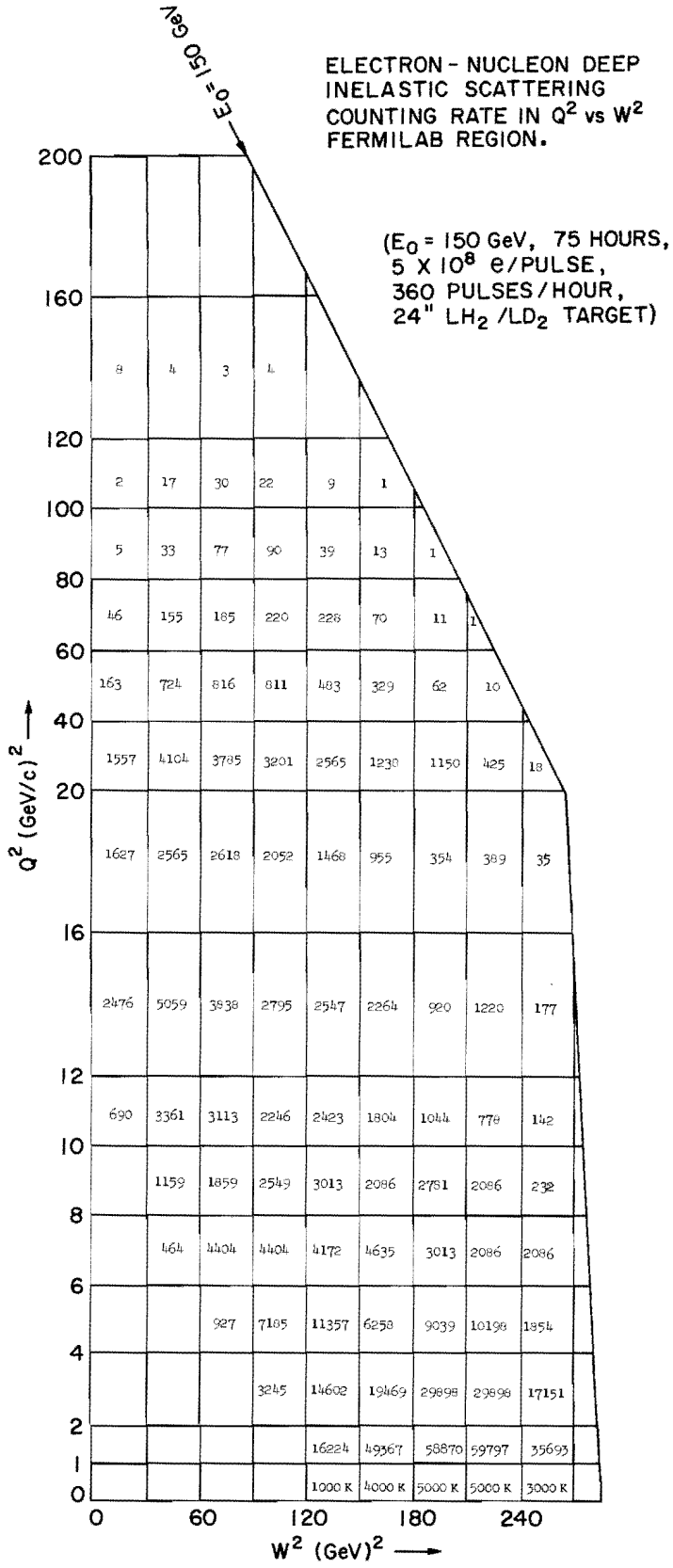
ELECTRON - NUCLEON DEEP INELASTIC SCATTERING COUNTING RATE IN Q^2 vs W^2 FERMILAB REGION.
(E_0 = 150 GeV, 75 HOURS, 5 X 10^8 e/PULSE, 360 PULSES/HOUR, 24" LH_2 /LD_2 TARGET)
E_0 = 150 GeV
Q^2 (GeV/c)^2
W^2 (GeV)^2
0 60 120 180 240
200 160 120 100 80 60 40 20 16 12 10 8 6 4 2 1 0
8 4 3 4
2 17 30 22 9 1
5 33 77 90 39 13 1
46 155 185 220 228 70 11 1
163 724 816 811 483 329 62 10
1557 4104 3785 3201 2565 1238 1150 425 18
1627 2565 2618 2052 1468 955 354 389 35
2476 5059 3838 2795 2547 2264 920 1220 177
690 3361 3113 2246 2423 1804 1044 778 142
1159 1859 2549 3013 2086 2781 2086 232
464 4404 4404 4172 4635 3013 2086 2086
927 7185 11357 6258 9039 10198 1854
3245 14602 19469 29898 29898 17151
16224 49367 58870 59797 35693
1000 K 4000 K 5000 K 5000 K 3000 K

FIGURE 11

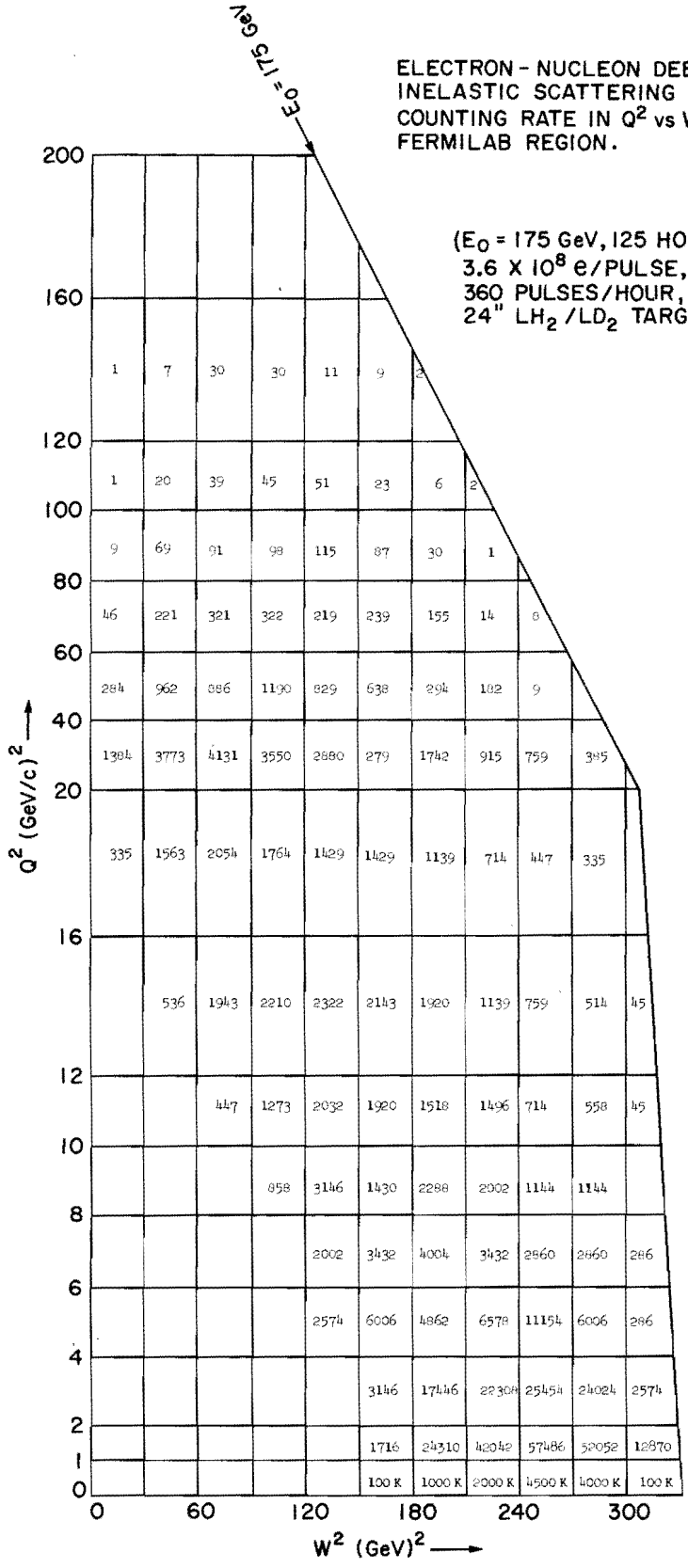
ELECTRON - NUCLEON DEEP INELASTIC SCATTERING COUNTING RATE IN Q^2 vs W^2 FERMILAB REGION.
(E_0 = 175 GeV, 125 HOURS, 3.6 X 10^8 e/PULSE, 360 PULSES/HOUR, 24" LH_2 /LD_2 TARGET)
E_0 = 175 GeV
Q^2 (GeV/c)^2
W^2 (GeV)^2
0 60 120 180 240 300
0 1 2 4 6 8 10 12 16 20 40 60 80 100 120 160 200
1 7 30 30 11 9 3
1 20 39 45 51 23 6 2
9 69 91 98 115 87 30 1
46 221 321 322 219 239 155 14 8
284 962 886 1190 829 638 294 102 9
1384 3773 4131 3550 2880 279 1742 915 759 385
335 1563 2054 1764 1429 1429 1139 714 447 335
536 1943 2210 2322 2143 1920 1139 759 514 45
447 1273 2032 1920 1518 1496 714 558 45
858 3146 1430 2288 2002 1144 1144
2002 3432 4004 3432 2860 2860 286
2574 6006 4862 6578 11154 6006 286
3146 17446 22308 25454 24024 2574
1716 24310 42042 57486 52052 12870
100 K 1000 K 2000 K 4500 K 4000 K 100 K

FIGURE 12

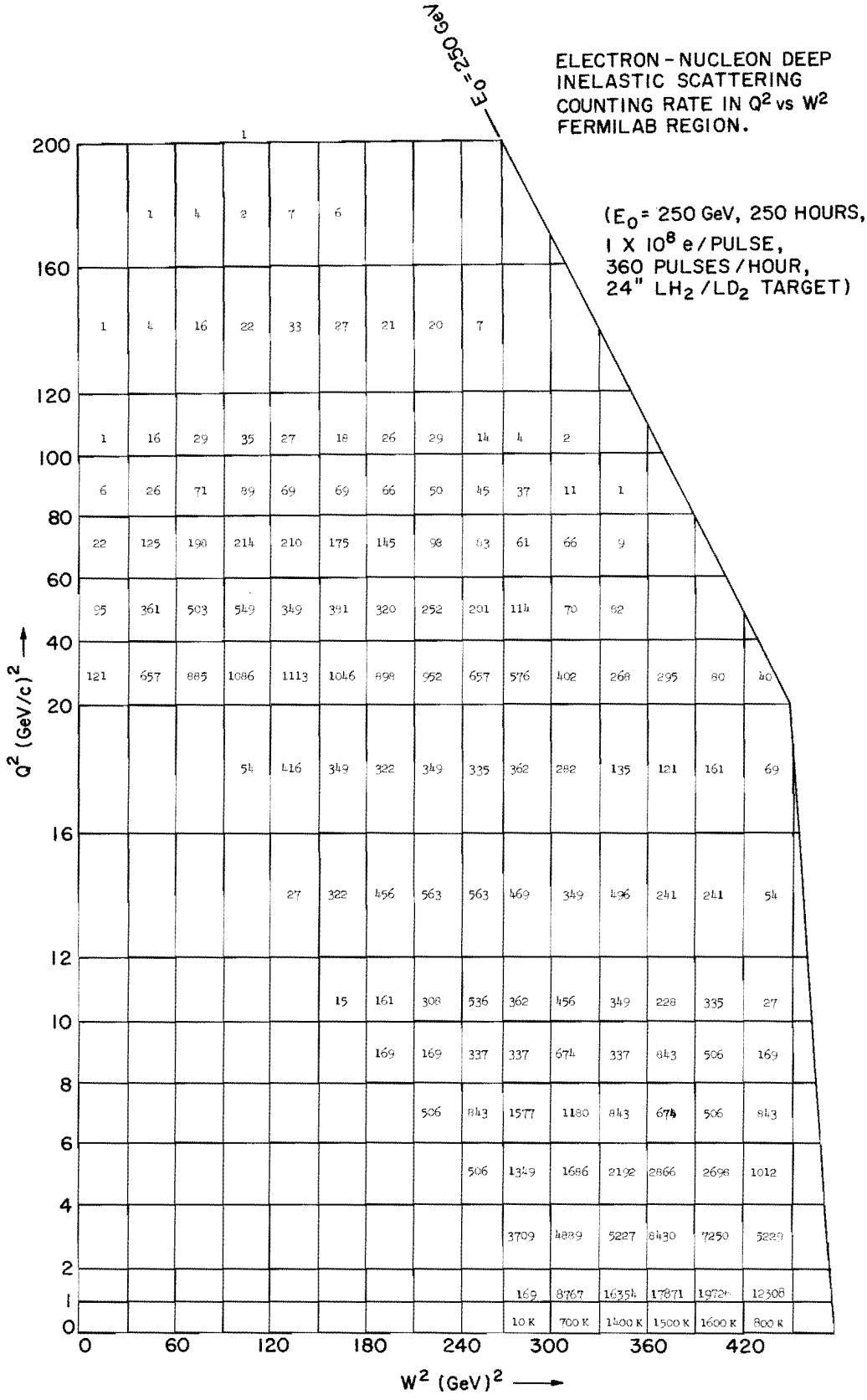
ELECTRON - NUCLEON DEEP INELASTIC SCATTERING COUNTING RATE IN Q^2 vs W^2 FERMILAB REGION.
(E_0 = 250 GeV, 250 HOURS, 1 X 10^8 e/PULSE, 360 PULSES/HOUR, 24" LH_2/LD_2 TARGET)
E_0 = 250 GeV
Q^2 (GeV/c)^2
W^2 (GeV)^2
0 60 120 180 240 300 360 420
200 160 120 100 80 60 40 20 16 12 10 8 6 4 2 1 0
1
1 4 2 7 6
1 4 16 22 33 27 21 20 7
1 16 29 35 27 18 26 29 14 4 2
6 26 71 89 69 69 66 50 45 37 11 1
22 125 198 214 210 175 145 98 63 61 66 9
95 361 503 549 349 391 320 252 201 114 70 92
121 657 885 1086 1113 1046 898 952 657 576 402 268 295 80 40
54 416 349 322 349 335 362 282 135 121 161 69
27 322 456 563 563 469 349 496 241 241 54
15 161 308 536 362 456 349 228 335 27
169 169 337 337 674 337 843 506 169
506 843 1577 1180 843 675 506 843
506 1349 1686 2192 2866 2698 1012
3709 4889 5227 8430 7250 5229
169 8767 16354 17871 19724 12308
10 K 700 K 1400 K 1500 K 1600 K 800 K

FIGURE 13

RADIATIVE CORRECTION IN DEEP INELASTIC ELECTRON - PROTON SCATTERING EXPERIMENTAL CROSS SECTIONS:

$$\frac{d^2\sigma(E_0)}{dW^2\,dQ^2} = \left\langle \frac{d^2\sigma(E_0)}{dW^2\,dQ^2} \right\rangle_{\text{MEASURED}} \times \delta(W^2, Q^2, E_0);$$

$$\delta(E_0, E', \theta_e) = \frac{\sigma\,(\text{INELASTIC})_{\text{THEORETICAL}}}{\sigma\,(\text{INELASTIC})_{\text{MEASURED}} + \sigma\,(\text{ELASTIC})_{\text{RADIATIVE TAIL}}}$$

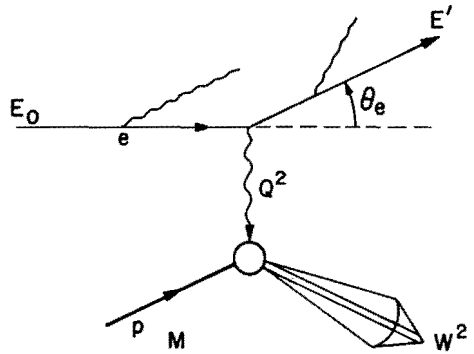

EXAMPLE CASE FOR INCIDENT ELECTRONS OR MUONS AT $E_0 = 175$ GeV AND $\theta_e = 2.5°$; ON 0", 12", AND 24" LH_2 TARGETS

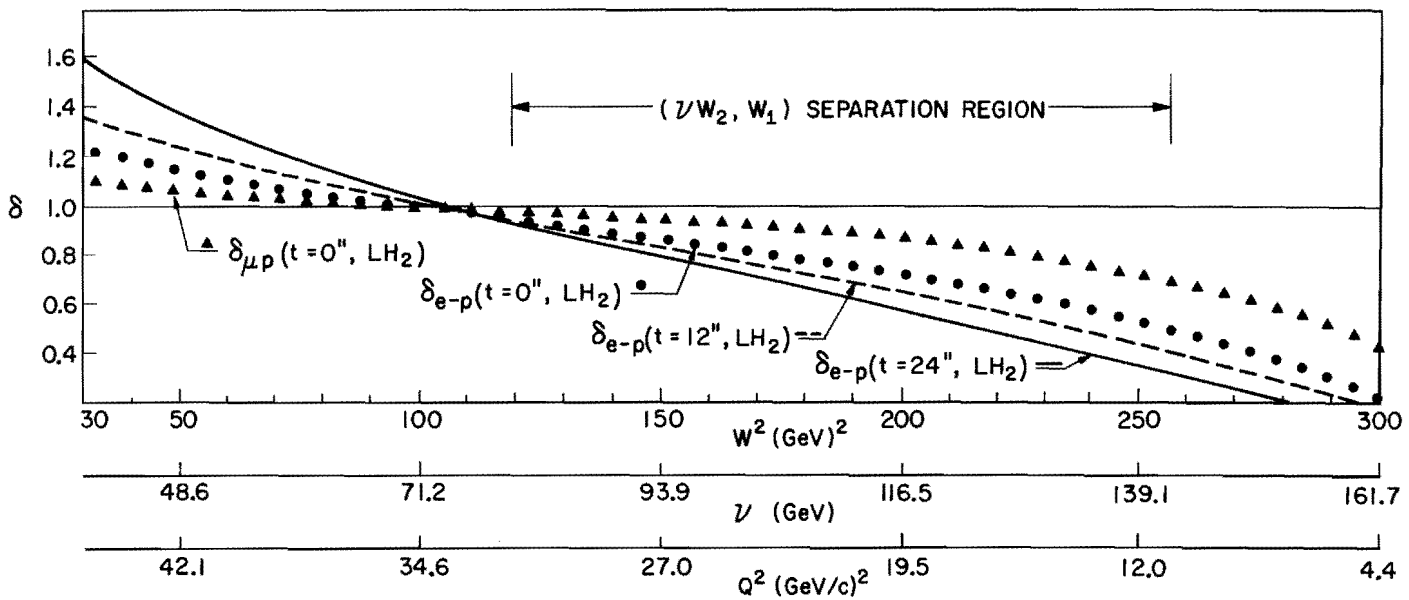

FIGURE 14

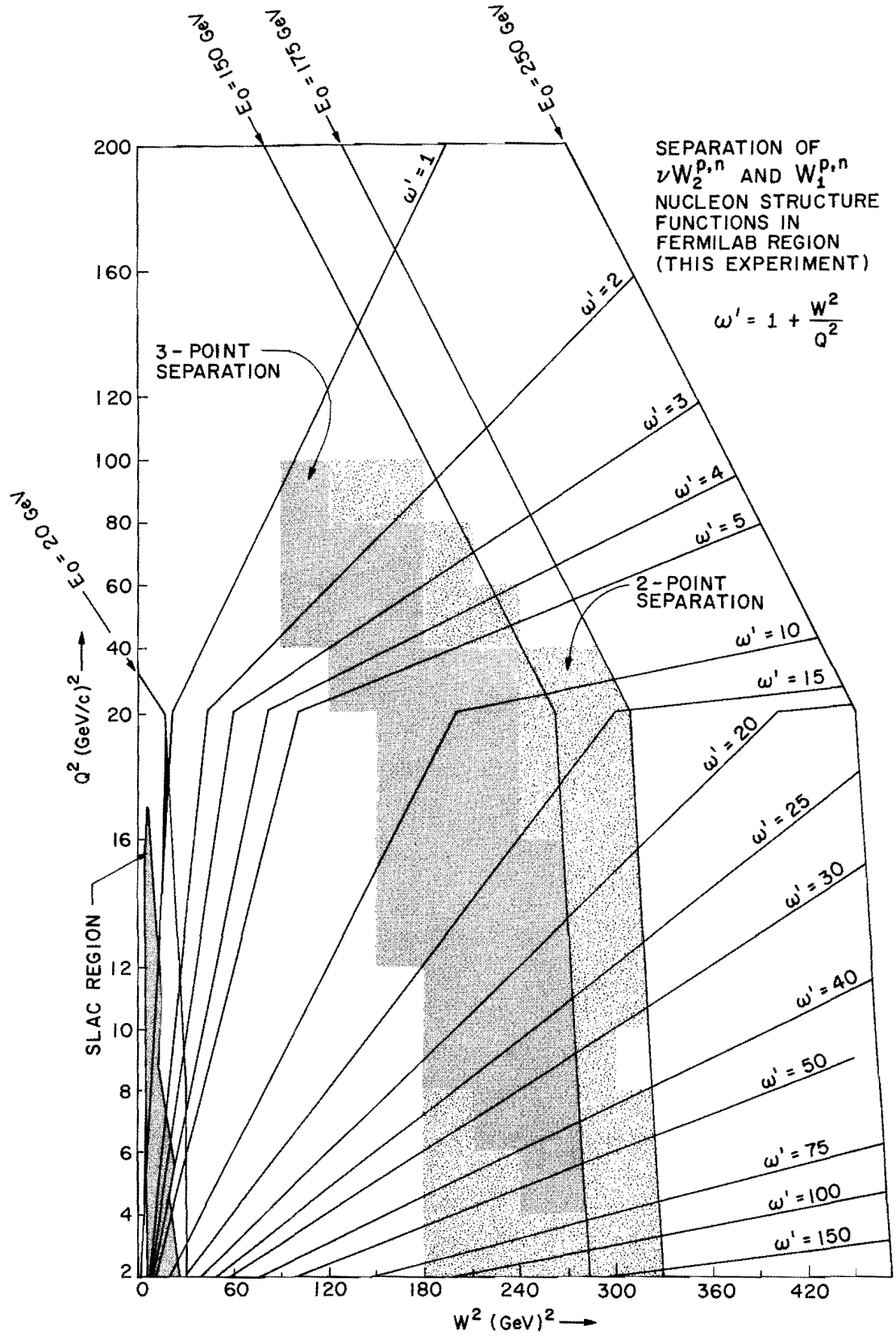
SEPARATION OF
$\nu W_2^{p,n}$ AND $W_1^{p,n}$
NUCLEON STRUCTURE
FUNCTIONS IN
FERMILAB REGION
(THIS EXPERIMENT)
$\omega' = 1 + \frac{W^2}{Q^2}$
E0 = 250 GeV
E0 = 175 GeV
E0 = 150 GeV
E0 = 20 GeV
ω' = 1
ω' = 2
ω' = 3
ω' = 4
ω' = 5
ω' = 10
ω' = 15
ω' = 20
ω' = 25
ω' = 30
ω' = 40
ω' = 50
ω' = 75
ω' = 100
ω' = 150
3-POINT SEPARATION
2-POINT SEPARATION
SLAC REGION
Q^2 (GeV/c)^2
W^2 (GeV)^2
200
160
120
100
80
60
40
20
16
12
10
8
6
4
2
0
60
120
180
240
300
360
420

FIGURE 15

EXPERIMENTAL SENSITIVITY TO A FORM OF SCALING BREAKDOWN

$$\nu W_1(Q^2,\nu) = \left(\frac{\Lambda^2}{Q^2+\Lambda^2}\right)^2 F_1^{e-p}(\omega')$$

$$\nu W_2(Q^2,\nu) = \left(\frac{\Lambda^2}{Q^2+\Lambda^2}\right)^2 F_2^{e-p}(\omega')$$

$$\omega' = 1 + \frac{W^2}{Q^2}$$

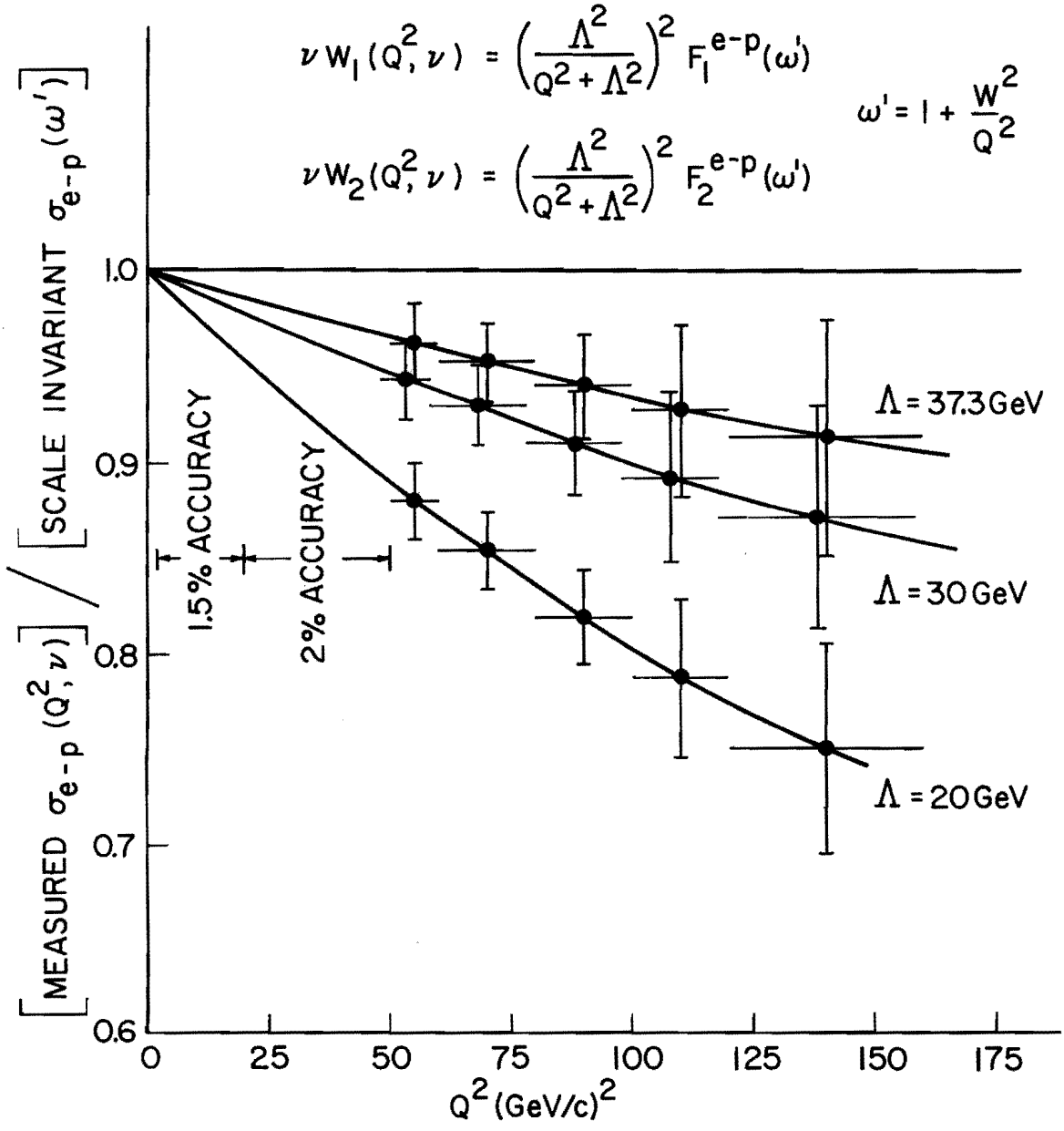

FIGURE 16

REFERENCES

(1) G. Miller, et al. Phys. Rev. D5, 528 (1972); W. B. Atwood, SLAC-185 (1975), R. E. Taylor, SLAC-PUB-1613 (1975); R. E. Taylor, Invited Talk presented at the 1975 International Symposium on Lepton and Photon Interactions at High Energies, Stanford University Stanford, California.

(2) a. Y. Watanabe, et al. Phys. Rev. Letts. 35, 898 (1975); C. Chang, et al. Phys. Rev. Letts. 35, 901 (1975);

b. L. W. Mo, Invited Talk presented at the 1975 International Symposium on Lepton and Photon Interactions at High Energies, Stanford University, Stanford, California.

(3) B. C. Cox, Proton-West High Intensity Secondary Beam Area Design Report, FERMILAB TM- (1975).

(4) Z.G.T. Guiragossián, 50-800 GeV, 10^8 - 10^{10} Pure Electron and Broad-Band Photon Beams at FERMILAB, HEPL Report No. 756 (1975); see also, Z.G.T. Guiragossián et al, P-193 Addendum, May 1975.

(5) Z.G.T. Guiragossián and R. E. Rand, Nucl. Instr. Meth. 107, 237 (1973).

(6) All technical questions were examined using detailed Monte Carlo techniques based on events acquired from a normalized sample of 5.84×10^4 pion beam tracks. We gratefully acknowledge the use of event data summary tapes from E-137, in which the 30" HBC at FERMILAB was exposed to 205 GeV π^- beam,

and 2500 inelastic multiprong events were acquired. In each event we regenerated multiple π^o tracks based on a real statistical description as to their multiplicity, angular distribution and momentum distribution, (assumed to be the same as those of π^+'s) such that their effective mass matched with the measured missing-mass. We thank Professors H. H. Bingham and W. B. Fretter for the use of analyzed events from the E-137 run.

(7) J. A. Appel, et al, FERMILAB-Pub-75/41 EXP.

(8) T. P. McPharlin, "Deep Inelastic π^o Electroproduction at 21 GeV and 13.5 GeV" (Ph.D. Thesis).

(9) Y. S. Tsai, "Radiative Corrections to Electron Scatterings," SLAC-PUB-848 (1971) and private communication.

(10) M. L. Perl et al, "Evidence for Anomalous Lepton Production in $e^+ - e^-$ Annihilation," SLAC-PUB-1626 LBL-4228 (1975).

PHYSICS OBJECTIVE

1. Do a clean deep inelastic electron scattering experiment; to measure and separate νW_2 and W_1 structure functions of protons and neutrons in all available kinematical regions beyond SLAC measurements.
2. Check scaling, check e-μ universality, check e^+-e^- differences.
3. Find exotic effects $(e^{\pm}\gamma)$, $(e^{\pm}\mu^{\mp})$, etc. in channels which are not accessible to SPS P-19 (Rubbia), μ + (45 m LH_2) experiment.
4. Our theoretician friends (Jim Bjorken and Alvaro DeRújula) recently advised us to concentrate also on acquiring data in the small ω' region, at $\omega' = 1 + W^2/Q^2 = 1 - 2$, to check for scaling behavior where the structure function $\nu W_2(\omega')$ is turning on — between $\omega' = 1 - 5$. This region is best covered with $E_{beam} = 50 - 75$ GeV . The beam intensity is highest, $(5 - 2) \times 10^9$ e/pulse and our apparatus acceptance is good in the region of interest. Our experimental resolution of $\Delta\omega'/\omega' = 3 - 4\%$ is excellently matched for such a study and, we have no rate or background limitations. Our studies of backgrounds show that the apparatus of E-192 can take beam rates of more than 10^{10} e/pulse.
5. Systematics in electron experiments are very different than in muon experiments. Also resolution, lepton identification and data analysis improves for electrons, therefore, it is important to do this electron experiment for an important number of results, even when there is a big CERN/SPS competition with muons.

We plan to implement the above physics objective with essentially the same beam hardware and experimental apparatus as in E-192. Changeover

in E-192/454 requires a few hours, therefore we can run these in interleaved periods of running time. The requested approval of #454 at this time is no different than the a priori approvals given for E-87/358 (Lee), E-203/391 (Kerth), E-300/325 (Cronin) and many others, where commonality of beam and equipment, and complementary physics goals are found. Approval of #454 at this time, will ensure that the required front-end beam hardware for electrons will develop. It will also provide the needed impetus for a strong collaboration to do E-192/454, with interested physicists from FERMILAB, Harvard University, Stanford University, the Yerevan Physics Institute and possibly Novosibirsk.

I. ELECTRON BEAM INTENSITY AND #454 RUN PLAN

The electron beam intensity estimates, as presented in Figure 2 of our proposal, are somewhat optimistic. We have traced the errors and find them to be in a) Proton-East to Proton-West beam acceptance scaling and b) 300 GeV to 400 and 470 GeV scaling. The errors occurred partly due to our lack of knowledge of an important measurement in the P-East beam at the point $E_p = 400$ GeV and $E_e = 90$ GeV .

Scaling of hadronic cross sections means that the invariant cross section:

$$f(x,p_\perp) \equiv Ed^3\sigma/dp^3 = \frac{1}{p_\ell^2}\frac{d\sigma}{d\Omega(dp/p)} , \quad x \simeq p_\ell/p_{max}$$

can be used to estimate yields according to the following relation:

$$Y \sim \frac{d\sigma}{d\Omega(dp/p)} \cdot [\Delta\Omega\,\Delta p/p]_{beam} = x^2 p_{max}^2\, f(x,p_\perp) \cdot [\Delta\Omega\,\Delta p/p]_{beam}$$

The yields thus obtained would be OK, provided that $(\Delta\Omega)_{beam}$ is less than the natural, hadronic production forward collimation, solid angle. However, it is found[3] that $(\Delta\Omega)_{natural} = 0.28\ (GeV^2\ str)/p_\ell^2$ for a symmetric (quadrupole triplet) acceptance beam. So that, at large x, $(\Delta\Omega)_{beam} > (\Delta\Omega)_{natural}$ and having more beam acceptance is no help. The result is a sharper fall-off in the yield curve at increasing values of x and p_{max}. The problem of having a variable effective angular acceptance is solved, by integrating the yield function at a given x and p_{max}, over the range of the angular acceptance of the beam, with a Monte Carlo generation technique. Thus, with the known qualities of

the P-East beam,[1] we reproduce the measured electron yield point at $E_p = 400$ GeV and $E_e = 90$ GeV, having as input the measured yield curve at $E_p = 300$ GeV. In the same way, and with the specified qualities of the P-West beam,[2] we compute an equivalent yield curve at $E_p = 300$ GeV. Both P-East and P-West yield curves at $E_p = 300$ GeV are shown in the attached figure; whereby we observe that in the P-West beam, the enhanced yield at small x is diminished at larger x. Using the same angular integration technique we compute the electron yield at $E_p = 470$ GeV. This curve is also shown in the attached figure.

We originally proposed running at electron energies of 150, 175 and 250 GeV. Based on the new yield curve, we now propose running at electron energies of 125, 150 and 200 GeV, where respectively, the intensities are: 9×10^8 e/pulse, 6×10^8 e/pulse, and 2×10^8 e/pulse from targeting of 10^{13} p/pulse at the P-West beam.

Qualitatively, there is not much difference in the coverage of large Q^2 regions between the old and new run plans. To first order, our kinematic region coverage is reduced by 15% - 20%. The Q^2 and W^2 scales in Figures 12, 13, 15 and 16 should be multiplied by the factor of 0.85. The $\nu W_2, W_1$ separation zone in Figure 15 now reaches to $Q^2 = 85$ (GeV/c)^2 and Q^2_{max} in Figure 16 becomes 130 (GeV/c)^2.

References: - 1. Proton-East tagged Photon Beam - a) P. Davis, et. al., FERMILAB TM-535 (1975); b) R. J. Morrison and F. V. Murphy, FERMILAB TM-633 (1976); c) T. Nash (private communications, May-June 1976).

2. Proton-West High Intensity Secondary Beam Area Design Report, B. Cox, et al. (1976).

3. G. Brianti, K. L. Brown, A. Placci, Proceedings of the 1973 International Conference on Instrumentation for High Energy Physics, Frascatti, p. 655.

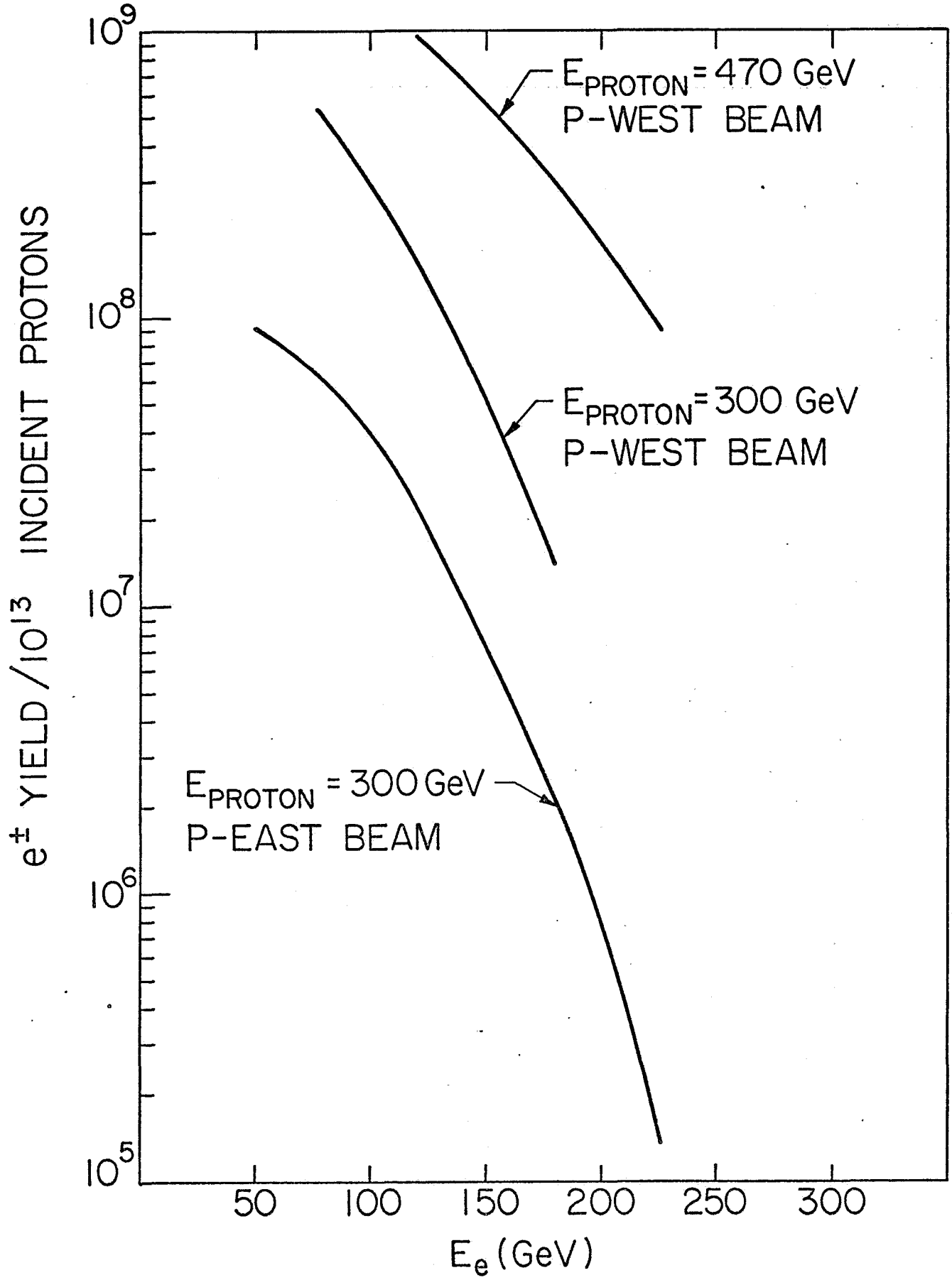
10^9
10^8
10^7
10^6
10^5
$e^{\pm}$ YIELD / 10^{13} INCIDENT PROTONS
E_{PROTON} = 470 GeV
P-WEST BEAM
E_{PROTON} = 300 GeV
P-WEST BEAM
E_{PROTON} = 300 GeV
P-EAST BEAM
50
100
150
200
250
300
E_e (GeV)

II. π/e RATIO OF THE ELECTRON BEAM

In the proposal (see page 9), we had wrongly interpreted that the π/e ratio immediately following the Pb radiator is 10^{-3}. With a π^- transmission of 30/10,000 in the beam, we felt that a π/e ratio of 3×10^{-6} was achievable. We have now computed and find an uper limit value of $\pi/e \leq 2.5 \times 10^{-2}$ immediately following the Pb radiator, with particle momenta and angles that could fall within the beam's initial acceptance. Therefore, the π/e ratio at the experimental target is 8×10^{-5} and we must work harder with synchrotron radiation energy loss and with intermediate collimations in the beam in order to reduce this ratio.

- We can do the experiment with $\pi/e = 4 \times 10^{-5}$ and we have found a way of achieving a $\pi/e = 8 \times 10^{-6}$, with minimal addition in beam hardware.

1. π/e Ratio at the Pb Radiator

We use the data in reference 1 to parameterize a neutron yield distribution in angles and momenta for the reaction: p + Be $\rightarrow$ n + anything, and a global parametrization [see D. C. Carey et. al., Phys. Rev. Letters 33, 330 (1974)] to describe the reaction: n + Pb $\rightarrow \pi^{\pm}$ + anything, at these energies. The beam's front-end is shown in Figure II.A. Within the known angular and momentum acceptance limits of the beam, and including target absorption and multiple scattering effects, we generate neutrons at the 16" Be target and charged pions at the 1/8" Pb radiator. The yield of π^- is obtained by a Monte Carlo calculation. The yield of electrons is known from our new and more conservative scaling calculation (see Section I). We find that for $E_p = 470$ GeV, and E_e in the range of 125 - 200 GeV,

the π/e ratio at the Pb radiator is $\leq 2.5\%$.

2. Required π/e Ratio at the E-192/454 Target

The required π/e ratio for #454 is defined by the rate of background electron detection from:

$$\pi^- N \rightarrow \pi^o + \text{anything} \qquad (a)$$

followed by Dalitz decay $\pi^o \rightarrow e^+e^-\gamma$ or $\pi^o \rightarrow \gamma\gamma \rightarrow e^+e^-$ giving a pair converted electron in the experimental target. This rate should be comparable with the rate of self-generated background electron detection from:

$$e^- N \rightarrow \pi^o + \text{anything} \qquad (b)$$

followed by $\pi^o \rightarrow e^+e^-\gamma$ and $\pi^o \rightarrow \gamma\gamma \rightarrow e^+e^-$ in the experimental target.

We have parameterized reaction (a) according to the data in reference 2, going out to transverse π^o momenta of 5 GeV/c. We have also parametrized reaction (b) using the μ-p data in reference 3. Using a Monte Carlo program, background electrons are propagated through the E-192/454 apparatus and detection rates are obtained in apparent (Q^2,W^2) bins. The distribution in Q^2,W^2 of background electrons from both processes is quite similar. The majority of background electrons fall in the lower right hand corner triangle with small apparent Q^2 and very large W^2. Data from this zone will be excluded in anyway, because radiative corrections obtain large amounts in this limited region (see Figures III.A and III.B).

By comparing the detected background electron rates from reactions (a) and (b) in Q^2,W^2 bins of acceptable data, we conclude that a π/e ratio in the beam of 4×10^{-5} is quite adequate; whereby the background from beam

pions does not exceed the self-generated background from beam electrons. Since background from both is symmetric in electron charge, our self-calibration experimental method will correct the data precisely for these effects.

3. A Way of Reducing the π/e Ratio to 8×10^{-6}

The layout of the magnetic elements of the beam is shown in Figure II.B, for the ultimate case of 1000 GeV/c operation and for the case of 300 GeV/c operation at beam turn-on time. There are four bend-points in the beam. Using just four magnets, one at each bend point, we are able to generate 2.7 GeV energy loss due to synchrotron radiation at 200 GeV; whereby from the Pb radiator 30 out of 10,000 π's arrive at the experimental target. By adding one extra magnet, over what is required for 300 GeV/c pion beam operation, we can form a +-+ chicane at the first bend-point, as seen in Figure II.B. The energy loss due to synchrotron radiation now becomes 7.8 GeV at 200 GeV. Moreover, we have now discovered four new locations along the beam, at places which are in between intermediate foci, where the use of half-collimators removes a fraction of the pion beam envelop, successively at all four sides. Thus, the net effect of the use of the one extra magnet and the four extra half-collimators is a π/e ratio of 8×10^{-6}. Having a chicane at the third bend-point is also helpful, but not as effective as the one at the first bend-point, because the lever arm between this chicane and the following intermediate x,y foci is shorter. The numbers in the proposal (see page 9) were derived by assuming chicanes at both the first bend and third bend-points, with $B_{max} = 36$ kgauss magnets. The 7.8 GeV energy loss value with chicane only at the first bend-point

is obtained with B_{max} = 44 kgauss magnets, as specified for 1000 GeV/c operation. The above results are obtained by a detailed ray tracing beam optics program.

References:

1. p + Be → n + anything, neutron yields — M. J. Longo et. al. UM HE 74-18, M-3 beam at 1 mrad; B. Knapp et. al., Phys. Rev. Letters 34, 1044 (1975), P-East Beam $\theta = 0^{o}$, [E-358]; p + p → n + anything at ISR, J. Engler et. al., Nucl. Phys. B84, 70 (1975).

2. $\pi^{-}p \rightarrow \pi^{o}$ + anything, G. Donaldson et. al., Phys. Rev. Letters 36, 1110 (1976), [E-268]; F. C. Winkelmann et. al., Phys. Rev. Letters 32, 121 (1974), and data summary tapes, [E-137].

3. μ-p → $h^{\pm}$ + anything, W. A. Loomis et. al., Phys. Rev. Letters 35, 1483 (1975), [E-98].

PRODUCTION OF ELECTRON BEAM AT FERMILAB

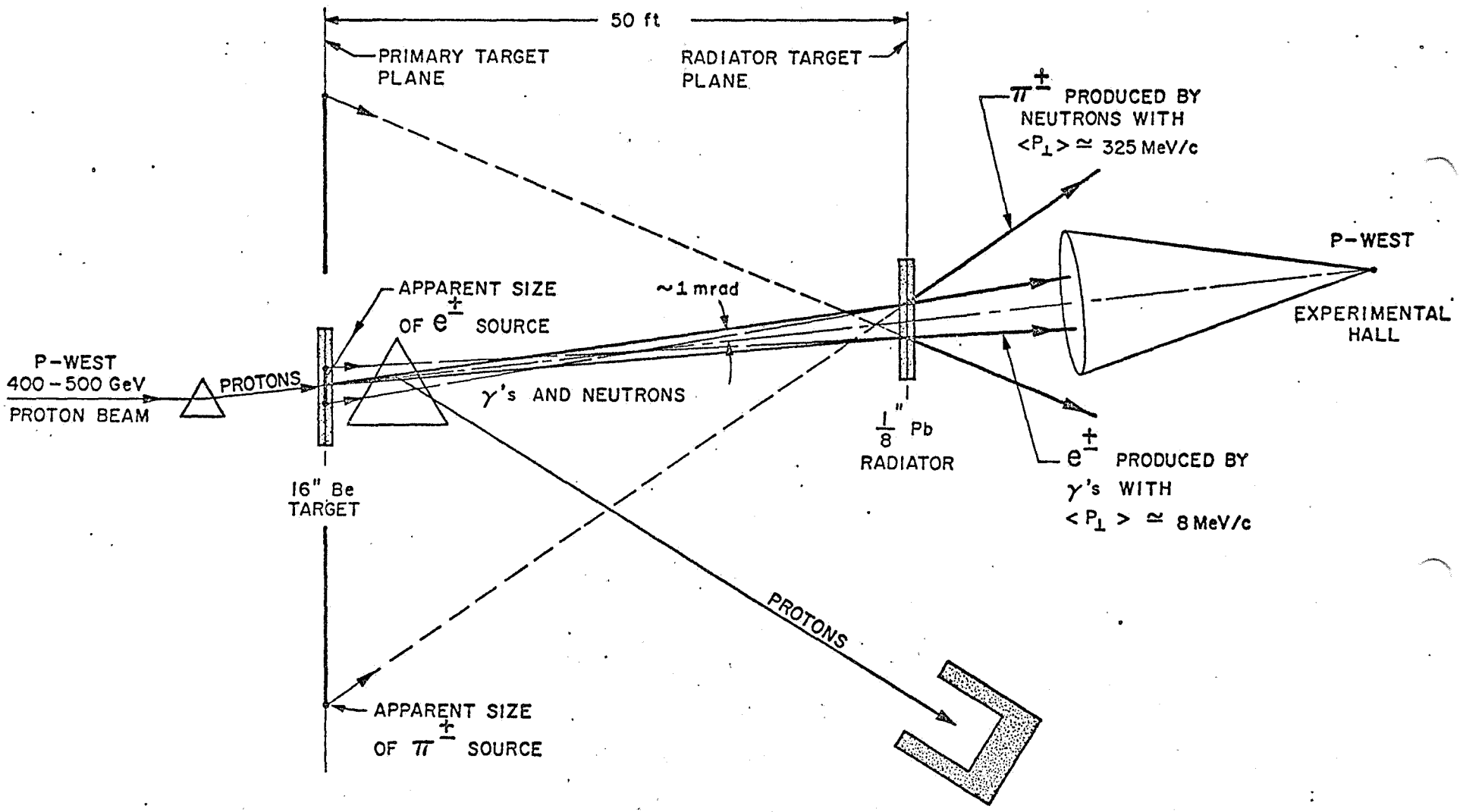

FIGURE II-A

FERMILAB PROTON-WEST SUPERCONDUCTING π/e BEAM

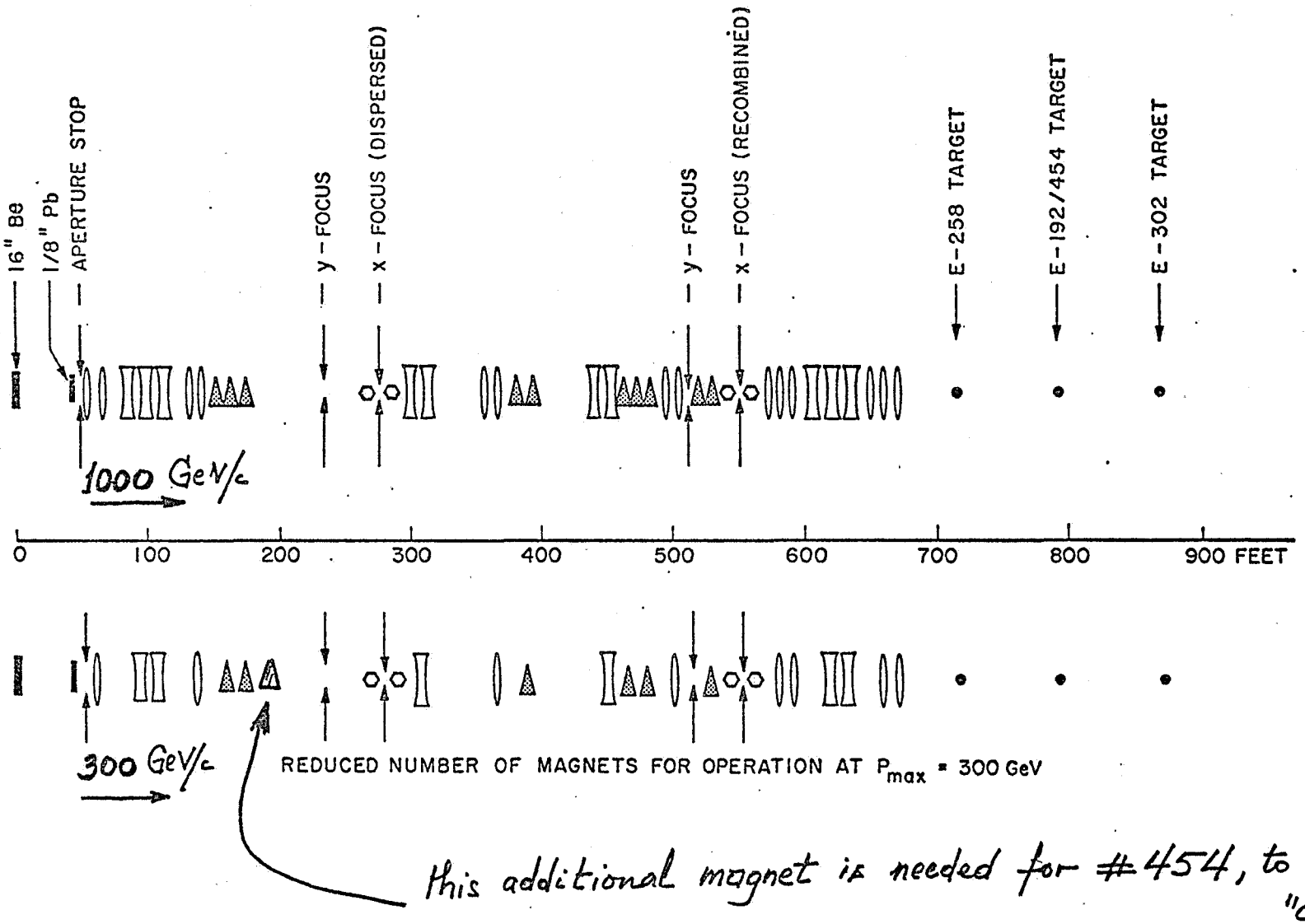

FIGURE II-B

III. RADIATIVE CORRECTIONS

Radiative corrections must be applied on data from electron-nucleon and muon-nucleon inelastic scattering experiments, to correct for radiative effects due to a) the internal bremsstrahlung before scattering and after scattering, b) the straggling of electrons in the target (LH_2/LD_2, windows, etc.), and c) the radiative tail from e-N or μ-N elastic scattering. As a function of E_o, E', θ_e, (incident and scattered electron energy, and scattering angle) the radiative corrections can be calculated exactly. However, in practice, in order to save computing time, the exact calculations are approximated by a formalism in which "angle peaking", "energy peaking" and "half-path-length" assumptions are made. It is found that peaking approximation calculations reproduce the exact calculation of radiative corrections with an accuracy of $\pm$ 3% on the average, and $\pm$ 5% in the worst case. This means, if the amount of radiative correction is say, 40%, the measured data will have a systematic uncertainty of $\pm$ 1.2% - $\pm$ 2% due to the peaking approximation. In #454, this uncertainty should be compared with the statistical uncertainty in each bin of (Q^2,W^2) which varies between 3% to 10%.

The experimental measurements $\sigma_{exp}(\text{inelastic})$ are equal to the sum:

$$\sigma_{exp}(\text{inelastic}) = \sigma_{radiated}(\text{inelastic}) + \sigma_{tail}(\text{elastic}) \quad .$$

So that, data in each bin of (E',θ_e) must be corrected by the amount δ:

$$\delta(E_o,E',\theta_e) = \frac{\sigma_{real}(\text{inelastic})}{\sigma_{radiated}(\text{inelastic}) + \sigma_{tail}(\text{elastic})} \quad ,$$

where σ_{real}(inelastic) is the true inelastic cross section, obtained theoretically with known νW_2 , $R = \sigma_L/\sigma_T$, and Q^2 dependence; $\sigma_{radiated}$(inelastic) is the calculated inelastic cross section with radiative effects folded-in; and σ_{tail}(elastic) is the calculated radiative tail from the e-p elastic scattering peak. Since σ_{real}(inelastic) must be known to obtain δ , an iterative procedure is required to evaluate the radiative corrections in a new kinematical region. This is described in the attached flow diagrams. For completeness, the procedure of obtaining e-n cross sections from measured e-D and e-p cross sections is also shown.

Figure III.A shows the (Q^2,W^2) kinematical region with lines of constant θ_e , at 1^o, 2.5^o, 5^o and 7^o. Using the radiative correction programs and formalism of Y. S. Tsai, we show, in Figure III.B, the amount of radiative corrections that must be applied on data falling on these lines. The use of 12" long LH_2/LD_2 target is assumed and the full radiative correction amounts, δ , are calculated for e-p and μ-p scattering.

- We conclude that:
  a) in the worst case, radiative corrections for e-p scattering are a factor of 2 more than the radiative corrections for μ-p scattering;
  b) at small θ_e , the radiative corrections are large, at small Q^2 and large W^2 values, dominated by radiation of electrons before scattering ($\delta < 1.0$);

c) at large θ_e, the radiative corrections become large, at very large Q^2 and small W^2 values, dominated by radiation of electrons <u>after scattering</u> ($\delta > 1.0$), however, in these extreme boundary regions the data rates are vanishingly small;

d) the radiative corrections have moderate values in the $\nu W_2, W_1$ separation zones.

- We propose to:

a) conservatively use 12" long LH_2/LD_2 target;

b) exclude data in zones where the amount of radiative correction is large. These zones are shown as shaded in Figure III.A, at the extreme boundaries. Data exclusion in the lower right-hand corner will also remove most of the detected electrons due to beam contamination π's which appear via $\pi^- N \rightarrow \pi^o$ + anything, followed by Dalitz decay $\pi^o \rightarrow e^+e^-\gamma$ giving an electron, or $\pi^o \rightarrow \gamma\gamma \rightarrow e^+e^-$ giving a pair converted electron.

The use of 24" long LH_2/LD_2 target would increase the amount of radiative corrections in the <u>accepted</u> regions by $\leq 26\%$. In general, target length, $T = L/X_o$, should be bounded by the requirements of

1) $T \leq 2t_{eq}$, $t_{eq} = \frac{3}{4}\frac{\alpha}{\pi}\left[\ell n\left(\frac{Q^2}{m_{\ell^2}}\right) - 1\right]$

and

2) $\frac{4}{3} T \leq 0.1$; the latter is needed in computer programs

due to the "half-path-length" approximation. A 24" LH_2/LD_2 target satisfies both of these requirements. We seek the advice of the PAC

members, in that perhaps we are being too conservative in the selection of target length.

Please note that radiative corrections, to first order, have no influence on experimental resolution. To second order, the radiative processes will change the statistical significance of each bin, by enhancement or depletion, by the factor $1/\delta$ where δ is given in Figure III.B. Fortunately, our ability to separate the structure functions is not influenced by radiative corrections in any harmful way. The radiative corrections in the very large Q^2 regions become significant, but those are regions where statistically significant data are not accessible.

We conclude this section by the following caution on systematic errors introduced by radiative corrections. The radiative correction is one of the most important sources of systematic error in the measurement of $R = \sigma_L/\sigma_T$, whether at $Q^2 \sim 10$ GeV/c^2 at SLAC, or at higher Q^2's in #454. In terms of amount of radiative correction, we are not much worse off than SLAC. In measuring R, we are comparing data at the same Q^2 and ν, firstly with low scattered electron energy, and then with an energy comparable to the incident one. A part of the radiative correction systematic error is cancelled in the comparison. The radiative corrections can be conveniently divided into two parts — radiation after scattering and radiation before scattering. As demonstrated in Figure III.B, radiation after scattering is the smaller of the two, and is approximately the same in each measurement. Therefore its systematic effect is cancelled. The radiation before scattering is large for the measurement where there is a low scattered electron energy.

The systematic effect of this part, therefore, does not cancel and becomes an error systematic on all measurements of R , from those at SLAC to the one in #454. We believe that the experience gained in SLAC experiments in making these corrections will enable us to minimize their systematic effects.

References:

a) Y. S. Tsai, "Radiative Corrections to Electron Scattering," SLAC-PUB-848 (1971) and computer programs;

b) L. W. Mo and Y. S. Tsai, Rev. Mod. Phys. 41, 205 (1969);

c) W. B. Atwood, "Electron Scattering Of Hydrogen and Deuterium at 50^{o} and 60^{o}" SLAC-185 (1975).

RADIATIVE CORRECTION FLOW CHART

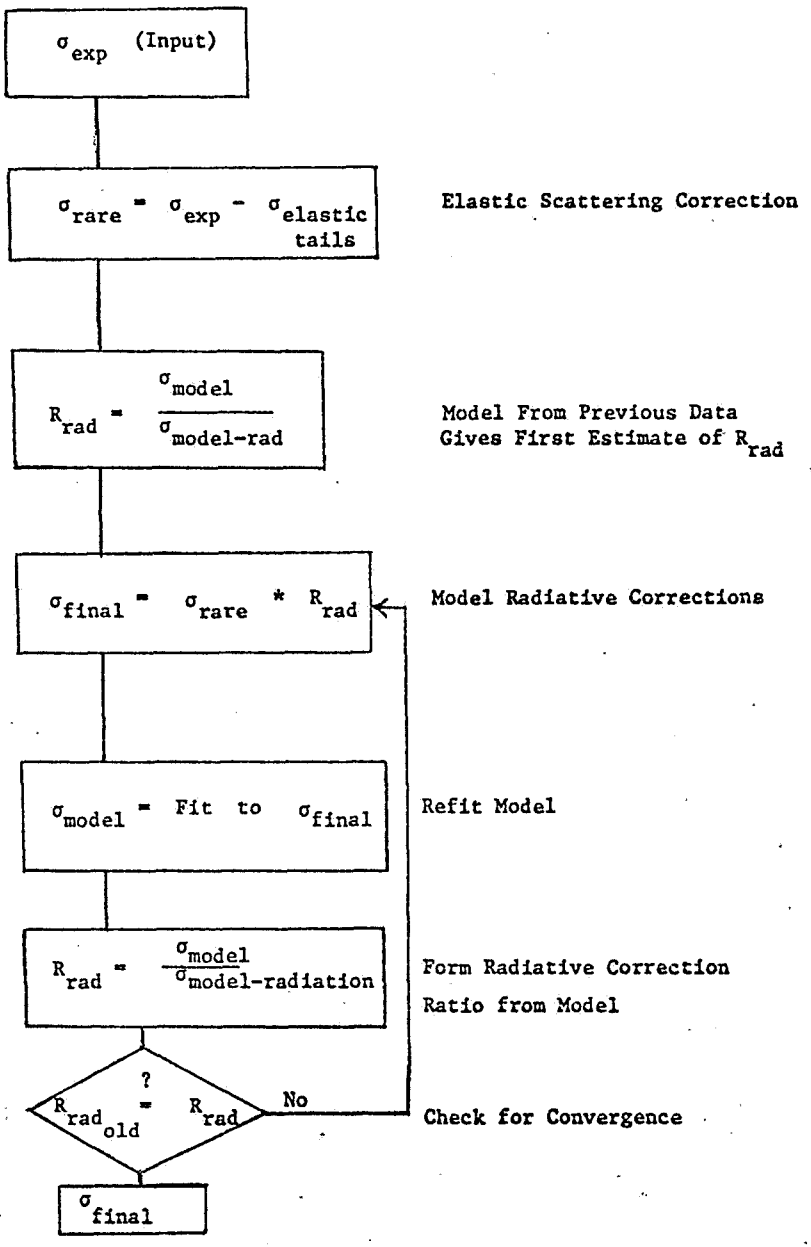

UNSMEARING FLOW CHART

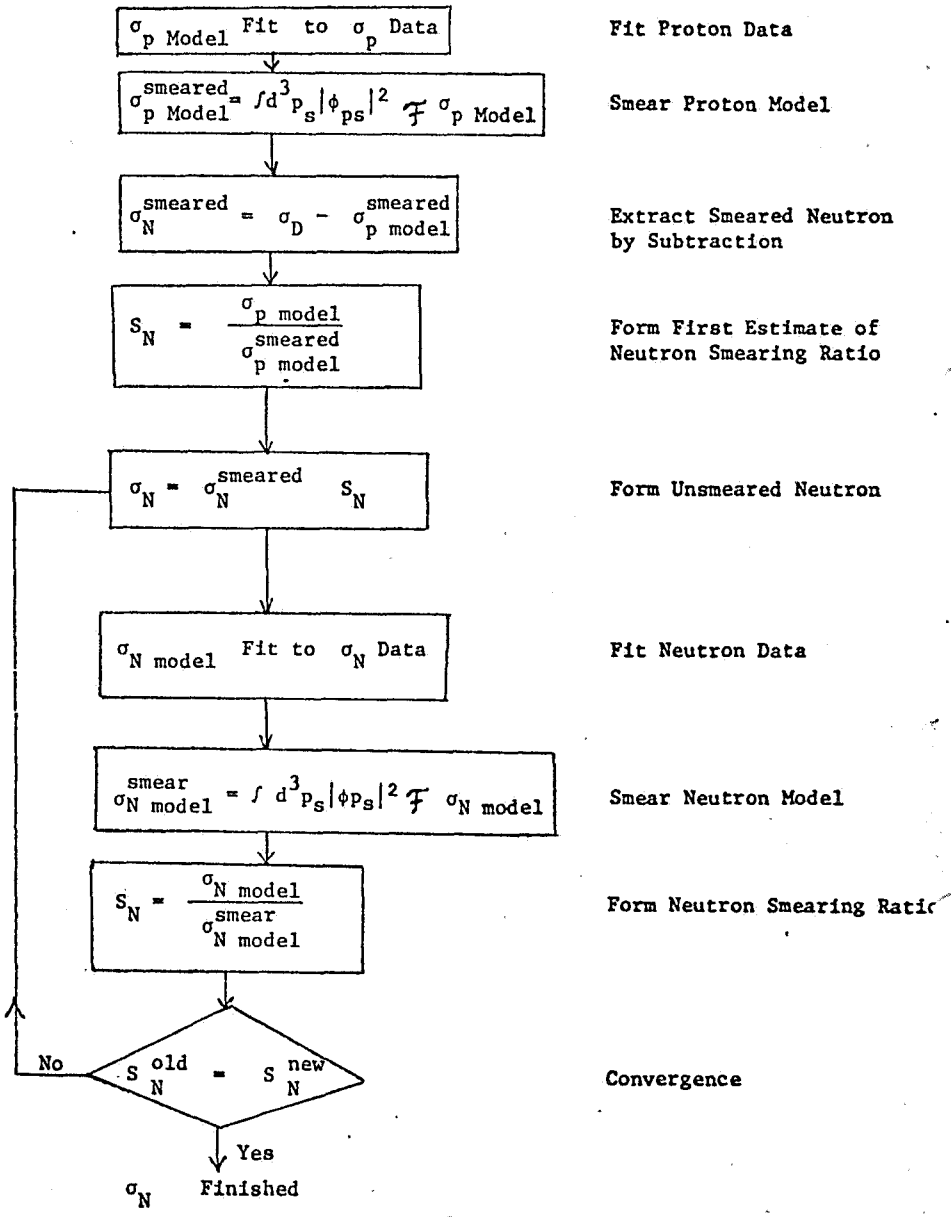

3364-4 (REV.A)

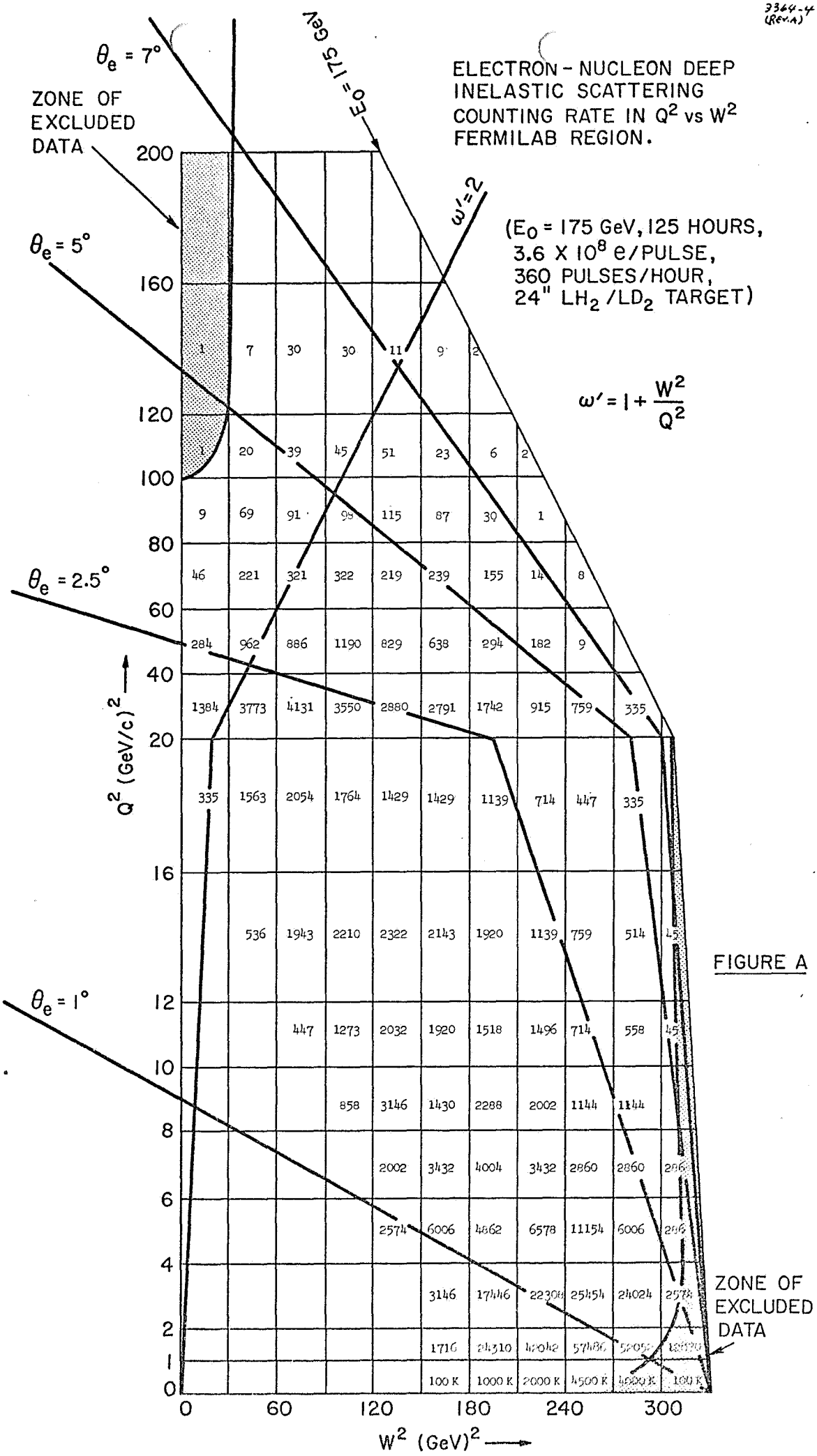

FIGURE A

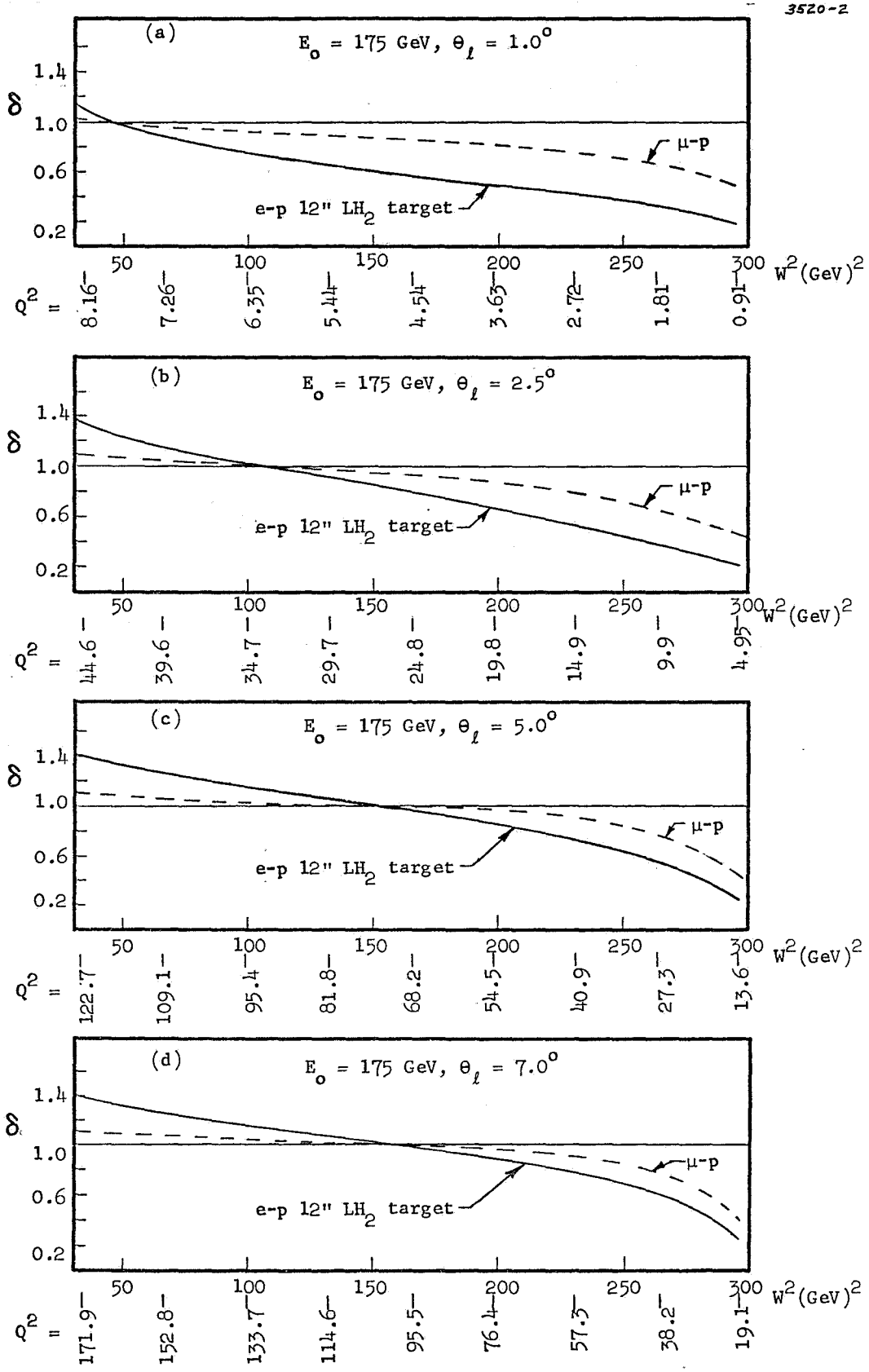
(a)
E_o = 175 GeV, θ_ℓ = 1.0°
δ
1.4
1.0
0.6
0.2
μ-p
e-p 12" LH_2 target
50
100
150
200
250
300
W^2(GeV)^2
ρ^2 = 8.16 7.26 6.35 5.44 4.54 3.63 2.72 1.81 0.91
(b)
E_o = 175 GeV, θ_ℓ = 2.5°
δ
1.4
1.0
0.6
0.2
μ-p
e-p 12" LH_2 target
50
100
150
200
250
300
W^2(GeV)^2
ρ^2 = 44.6 39.6 34.7 29.7 24.8 19.8 14.9 9.9 4.95
(c)
E_o = 175 GeV, θ_ℓ = 5.0°
δ
1.4
1.0
0.6
0.2
μ-p
e-p 12" LH_2 target
50
100
150
200
250
300
W^2(GeV)^2
ρ^2 = 122.7 109.1 95.4 81.8 68.2 54.5 40.9 27.3 13.6
(d)
E_o = 175 GeV, θ_ℓ = 7.0°
δ
1.4
1.0
0.6
0.2
μ-p
e-p 12" LH_2 target
50
100
150
200
250
300
W^2(GeV)^2
ρ^2 = 171.9 152.8 133.7 114.6 95.5 76.4 57.3 38.2 19.1

FIGURE B